Effect of Series Resistance Increase on Fill Factor of PV Cells Extracted from Field Aged Modules of Different Climates

by

Abhishiktha Tummala

A Thesis Presented in Partial Fulfillment
of the Requirements for the Degree
Master of Science

Approved July 2016 by the
Graduate Supervisory Committee:

Govindasamy Tamizhmani, Co-Chair
Phelan Patrick, Co-Chair
Liping Wang

ARIZONA STATE UNIVERSITY

August 2016

ABSTRACT

Solar photovoltaic (PV) industry is tipped to be one of the front-runners in the renewable industry. Typically, PV module manufacturers provide a linear or step warranty of 80% of original power over 25 years. This power loss during the field exposure is primarily attributed to the development of performance affecting defects in the PV modules. As many as 86 different defects can occur in a PV module. One of the major defects that can cause significant power loss is the interconnect metallization system (IMS) degradation which is the focus of this thesis. The IMS is composed of cell-interconnect (cell-ribbon interconnect) and string-interconnect (ribbon-ribbon interconnect). The cell interconnect is in turn composed of silver metallization (fingers and busbars) and solder bonds between silver busbar and copper ribbon. Weak solder bonding between copper ribbon and busbar of a cell results in increase of series resistance that in turn affects the fill factor causing a power drop. In this thesis work, the results obtained from various non-destructive and destructive experiments performed on modules exposed in three different climates (Arizona - Hot and Dry, Mexico - Warm and Humid, and California - Temperate) are presented. These experiments include light I-V measurements, dark I-V measurements, infrared imaging, extraction of test samples from the modules, peel strength measurements and four-point resistance measurements. The extraction of test samples was performed using a mechanical method and a chemical method. The merits and demerits of these two methods are presented. A drop of 10.33% in fill factor was observed for a 0.05Ω increase in the series resistance of the modules investigated in this work. Different combinations in a cell that can cause series resistance increase were considered and their effect on fill factor were observed using four-point probe

experiments. Peel test experiments were conducted to correlate the effect of series resistance on the ribbon peel strength. Finally, climate specific thermal modelling was performed for 4 different sites over 20 years in order to calculate the accumulated thermal fatigue and also to evaluate its correlation, if any, with the increase of series resistance.

Dedicated to my beloved parents, Nagendra Kumar Tummala and Sri Lakshmi, my sister Abhigna and all other family members and friends who made me what I am with their constant support and encouragement.

ACKNOWLEDGMENTS

First, I would like to thank my professor Dr. Govindasamy Tamizhmani for giving me this wonderful opportunity to work under him at Photovoltaic Reliability Laboratory. His continuous support, constant encouragement and his valuable inputs to my work irrespective of his busy schedule have been invaluable to my work and me. I would also like to thank Dr. Nick Bosco of National Renewable Energy Laboratory for his valuable inputs during my visit to NREL and constantly clarifying my queries whenever requested. Some of the results presented in this thesis are based on the modules provided by UNAM (National Autonomous University of Mexico). The kind support of UNAM is gratefully acknowledged. I would also like to thank my colleagues who worked with me especially Mr. Sai Tatapudi, our technical lab manager, Christopher Raupp, Darshan Chowdary and Srinivas Mantha for helping me out with my experiments whenever I requested help. Finally, I would like to thank the lord almighty for making all this happen.

Thank you all. Thanks a ton.

TABLE OF CONTENTS

Page

CHAPTER Page

CHAPTER Page

LIST OF TABLES

Table Page

LIST OF FIGURES

Figure Page

Figure Page

Figure Page

Figure Page

1.0 INTRODUCTION

1.1 Background

Solar photovoltaic (PV) technology is one of the major alternative energy technologies. Solar cells generally are high current and low voltage generating devices. Currently, the largest cell area is around 15.6 x 15.6 cm^2 [1]. With increase in cell size and hence the current, the length and number of the busbars and fingers also increased over the years. One of the major sources of power loss in field exposed solar cells is the increase in the series resistance (R_S). The main reason for the cause of increased series resistance is solder bond degradation. As a module is exposed in the field, depending on the climatic conditions, the thermomechanical fatigue or cracks develop in the solder bonds leading to increased series resistance.

Previous studies show that modules when exposed in the field undergo thermomechanical fatigue which results in changes in the solder-joint geometry thus causing in the reduction in the number of redundant solder joints in a module thus reducing the performance [2]. This change in solder geometry and accumulated fatigue can be directly attributed to the increased series resistance in the electrical circuit of a solar cell [3]. It was also studied that parasitic resistances such as series and shunt resistances are detrimental to the performance of a solar cell. It was reported that increase in series resistance attributed to 50% drop in the power of a module after an exposure of 130 kWh/m^2 [4]. Hence a standard procedure needs to be developed in order to understand the relationship between the solder bond fatigue, series resistance between various components of a solar cell and the thermomechanical fatigue.

1.2 Statement of the Problem

It is known that the solder bond fatigue increases the series resistance which in turn results in fill factor drop and hence power loss. So it is important to understand how climatic conditions affect the solder bond strength and hence the series resistance. Different possible combinations where the series resistance were most likely to occur were calculated in order to understand which part of a solar cell contributes more in series resistance in a particular climatic condition.

1.3 Objective

The main objective of this work is to calculate the series resistance for various cell circuit combinations in a solar cell. These experiments were conducted for modules from three different climatic conditions. The cells were cut from the modules, encapsulant was chemically dissolved, glass pieces were removed, the resistance measurements were performed on the IMS (interconnect metallization system) and the calculations were performed. After the calculations, peel test experiments were performed to determine the bond strength between aged and fresh samples. Using coring procedure, samples were removed from various modules and were observed under SEM to understand the composition of the solder and to observe any cracks present in the solder joints. The main objective of this work is shown in the flow chart below.

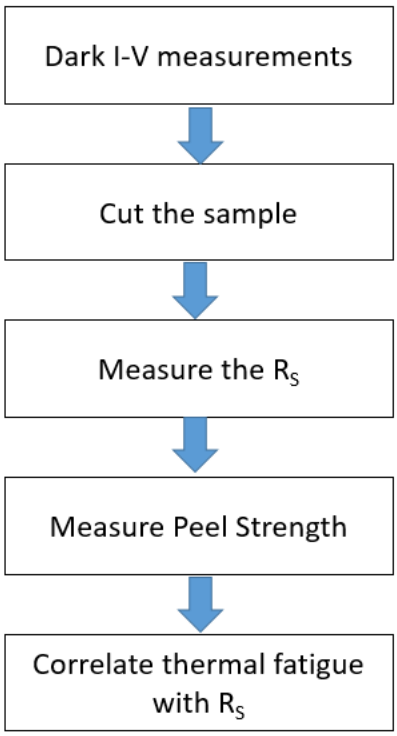

Figure 1: Objective of Thesis Work

2.0 LITERATURE REVIEW

2.1 Effect of Solder Bond Fatigue in PV Module

Oh et al [5] have investigated the migration of Sn and Pb lead solder on to the Ag fingers (busbars) in a crystalline silicon module exposed for 6 years. Typically, accelerated tests are performed to observe if the PV modules are reliable over the span of 25 years. Damp heat are generally performed in order to identify different modes of solder bond degradation in a PV module. To understand various degradation modes, the samples were obtained using coring procedure and were observed under SEM. It was observed that due to repeated thermal cycles and the delamination, moisture infuses through the module that result in galvanic corrosion, which leads to the migration of Sn and Pb on to the Ag busbars. In addition, it was observed that solder bond cracking and reduction in the amount of solder leads to increase in series resistance. Quintana et al [2] have studied the various types of most commonly observed degradations in a PV module. They identified interconnect degradation as one of the common type of degradation where the effects lead to increased series resistance, increased heating in the module and localized hot spots causing burns in the backsheet, solder joints or the encapsulant. Interconnect degradation occurs when the cell to ribbon and the ribbon-to-ribbon area changes in their grain structure or geometry. This generally happens due to the coarsening of grains in the solder bond, which would eventually lead to solder joint failure. They also state that the thermomechanical fatigue that occurs over the years causes the solder bond to crack which leads to the increase in series resistance as the current is forced to circulate through the remaining limited non-damaged solder joint area.

King et al [3] performed a detailed metallurgical analysis on the solder bonds in order to understand their degradation. Coring procedure was used in order to extract samples from both field aged and fresh samples. When observed under SEM it was seen that, as a module is in the field continuously, the solder bonds age due to continuous thermal cycling and the expansion and contraction in solder bonds cause the solder bonds to develop more fatigue and hence become brittle and dissociate into large grains of Sn and Pb. This process hence leads the solder bond to crack and hence develop high resistance to current transfer in the module.

2.2 Effect of Series Resistance on PV Module Performance

Kim et al [6] studied on the mitigation methods for solder corrosion for c-Si photovoltaic modules. In their study they observed that the solder bond corrosion poses serious difficulties to the outdoor exposed PV modules and the degradation of the solder bond mainly effects contributes to the increase in the series resistance (R_S) of the PV module. After experiments, it was revealed that the main reason for the decrease in power of the PV module is the drop in Fill Factor (FF), which is attributed to the increase in R_S. Jaya Krishna and Tamizhmani [7] performed a statistical analysis on the various cell parameters which are responsible for the power degradation of a power plant in a hot-dry climate. It was observed that the two major sources of power degradation are FF and I_{SC} drops. The Fill Factor drop is attributed to the series resistance increase caused by the solder bond degradation whereas the I_{SC} drop is attributed to the optical transmission loss caused by the encapsulant discoloration.

King et al [3] have worked on the photovoltaic module performance following a long-term exposure in the field. They indicate that the series resistance present in wiring, junction-box terminations, cell-interconnect ribbons, cell metallization, emitter and base regions of solar cells, and cell solder bonds results in operating voltage losses, which limit the ultimate performance of a photovoltaic system. A decline in the power output of about 0.5%/year can be seen as the series resistance accumulates over years of exposure.

2.3 Calculation of Series Resistance of a Module

According to King et al [3] it takes several years before the influence of series resistance on the system level performance can be detected. However, in a module level, a better way of quantifying the results of increased series resistance would be by the dark I-V measurements. Various authors have developed different equations in order to measure the series resistance of a module more effectively [1, 8-12]. In general, the series resistance is calculated by using the following equation

$$I = I_L - I_o e^{\frac{q(V+IR_S)}{nkT}}$$

Where I_L is the light generated current, I is the cell output current, V is the voltage across the cell terminals, T is the temperature, q and k are constants, n is the ideality factor, and R_S is the cell series resistance [13].

2.4 Climate Specific Thermal Modelling

According to a recent survey in India [14], it was observed that the modules deployed in hot climates exhibited higher power loss due to increased series resistance whereas in relatively cooler climates, the power degradation was not effected significantly by

increase in series resistance. To tackle this problem, Bosco et al [15] came up with a finite element model in order to perform simulations of Pb-Sn solder thermomechanical fatigue for seven different cities of different climatic conditions. In order to understand the influence of weather on the solder damage accumulation, an empirical model was developed in order to calculate the damage using specific weather inputs. This empirical model depends on three meteorological factors and they are the mean maximum daily temperature, daily temperature change and a characteristic of clouding events that is the number of reversals over a specific reversal temperature. Using these factors, the damage was calculated for all the seven cities over a period of one year for a rate of 1-minute intervals. These results when compared to those of FEM simulations showed very good correlation.

3.0 METHODOLOGY

3.1 Module Selection

In this work, modules from three different climates were secured and evaluated. They are hot and dry (Arizona), warm and humid (Mexico) and temperate (California). Two modules from Arizona which are eighteen years old and a control module (unstressed), one twenty-eight year exposed module and a control module from California and a twenty-three year-old exposed module from Mexico were used for evaluation in this work.

3.2 Non-Destructive Testing

The following nondestructive techniques utilized were utilized in this work: current-voltage measurement (I-V), visual inspection (VI), diode failure (DF), infrared (IR) imaging, electroluminescence (EL) imaging, UV fluorescence (UVF), dark I-V (D-I-V), module level quantum efficiency (M-QE), and module level reflectance spectroscopy (M-RS). Since the purpose of most of these techniques is commonly known, it is explained only very briefly in this section. The test sequence that was based on the characterization tests performed by Matthew Chicca [16].

3.2.1 Current-Voltage (I-V) Measurements

The I-V data was collected using a Daystar I-V curve tracer under natural sunlight. One monocrystalline silicon reference cell and one polycrystalline silicon reference cell were used during data collection to ensure accurate readings. To monitor the temperature of the module, a thermocouple was attached to the center of each module and an additional thermocouple was used to measure the ambient temperature. The degradation rates of

individual modules were determined, along with the temperature coefficients based on the I-V data and the number of years of field exposure. The light I-V based series and shunt resistances were also calculated.

3.2.2 Visual Inspection (VI)

All the modules were inspected using the visual inspection checklist[17] developed by National Renewable Energy Laboratory (NREL). The conditions of the modules were visually and photographically examined to determine the visual defects or failures.

3.2.3 Diode Failure (DF)

A diode checker was used to check the diode functionality (open circuit or short circuit). If diodes fail in the short-circuited mode it will lead to the power loss and if they fail in the open-circuited mode modules could lead to fire hazard or electrical safety issue. A line checker was used to check the functionality of the diode. The module was connected to the current generator and a small amount of electricity was passed through it and the test is then started. If there results no beeping sound when module is not shaded, then that particular string was being bypassed resulting from another issue. If the module was being shaded and a beep was heard than the diode was not working properly because that string should have been bypassed.

3.2.4 Infrared Imaging (IR)

In this test, the modules were placed outside and put under short circuit or loaded conditions. This test's main purpose is to check for hotspots if any, present in the module. Hotspot cells within the module are defined as the cells that are operating at or above 20°C higher than the average temperature of all the cells within the module. These

hotspots could eventually lead to accelerated power degradation or safety failures including backsheet delamination or burning and solder bond issues. Each module after being connected was left outside for around 10 minutes and an image was taken using Fluke Tir2 Ft Thermal Imager camera, the images were processed and altered using Smart View software to more clearly highlight the areas of interest.

3.2.5 Electroluminescence Imaging (EL)

Semiconductors in photovoltaic modules usually convert light into electrical energy, however due to their unique properties if the process is applied in the reverse order semiconductors will produce light as excess electrons are excited up to the conduction band. This phenomenon is known as electroluminescence and it serves as a useful tool for module characterization. An external power supply is connected to a module and a voltage and current up to 1.33*the measured Isc value is applied to the module in a dark room under forward bias conditions in order to identify areas of cell in a module where current is not reaching easily or at all. A Sensovation HR-830 pro camera was used on a 30-second exposure time to obtain the EL images. The modules being investigated had junction boxes on opposite ends so special attention was given to ensure that the positive side junction box was always placed on the left side of the image. Once the high resolution images were captured details such as cell cracks, cell shunting and cell metallization adhesion issues were able to be seen.

3.2.6 Dark I-V (D-I-V)

The dark I-V measurements were carried out indoor under controlled temperature conditions to obtain dark series and shunt resistances measurements. Dark I-V measurements are very much useful in solder bond reliability experiments.

3.2.7 Module Level Quantum Efficiency (C-M-QE)

to obtain QE losses in the shunted regions (if any based on EL imaging), heavily browned encapsulant cell center regions and clear cell edge regions, a non-destructive cell-module QE (C-M-QE) was performed using PV measurement's Solar Panel Quantum Efficiency Measurement System model QEX12M. In addition to the edge of cell and center of cell comparison within a module, center of cell measurements was compared between control modules and their respective aged modules. These measurements were performed at various spots of individual cells without cutting the back sheet of the module.

3.2.8 Module Level Reflectance Spectroscopy (M-RS)

A field spec 4 wide res spectroradiometer was used, to measure the reflectance of both control and field aged modules. The data was processed using view spec pro software and graphed in excel. By combining the C-M-QE technique with nondestructive module level reflectance spectroscopy technique, the influence wavelength-dependent encapsulant discoloration on short circuit current can be understood.

3.3 Backsheet Cutting

In order to perform cell level I-V tests, the soldering of the ribbons from each individual cell is required. In order to do that, the backsheet of each cell in the module needs to be cut. Firstly, all the areas where the module has to be cut in every cell are marked. Using a

heat gun, the marked area is exposed for a minute and the marked part is cut out using a heavy duty razor blade. Heating the backsheet loosens up the encapsulant (EVA- Ethyl Vinyl Acetate) hence making easier to remove it.

3.4 Soldering

Once the backsheet is cut, the ribbons from each cell have to be soldered so that they can be attached to the probes of the cell level I-V tester. In order to solder, the ingredients required are solder gun, flux pen in order to remove the oxides and fasten up the soldering process and ribbon. Figures 2 and 3 show the soldering equipment and the backside of the cell after soldering.

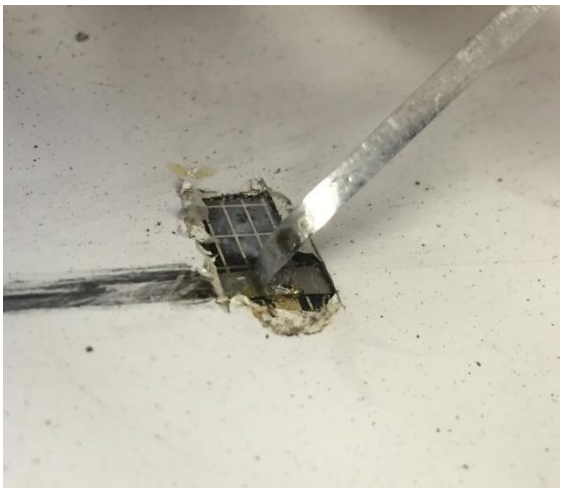

Figure 2: Soldered Ribbon On the Backsheet of PV Module for Dark I-V Measurements

Figure 3: Solder Flux, Ribbon and Gun

3.5 Cell Level I-V curves

Once the soldering procedure is completed for all the possible cells in the module, cell level I-V curves are taken for each cell possible. In a module, each ribbon runs a length

of about 2 cells. It starts from either top/bottom of the cell and ends at bottom/top of the next cell. So, when a particular cell's I-V curve is being taken, the bottom ribbon of the cell is the positive side of the cell and the top part of the ribbon which runs all the way to the bottom of the next cell is the negative side of the cell. The probes are connected to the soldered ribbons, two probes (red) to the positive and two probes (black) to the negative. The light source is brought above the cell whose I-V is being measured and the light I-V is measured using the software provided by the manufacturer and then the cell is covered by the opaque sheet and the dark I-V curves are taken. Figures 4 and 5 show the indoor solar simulator used and how the light beam is focused on the cell for whom the I-V curve is being measured.

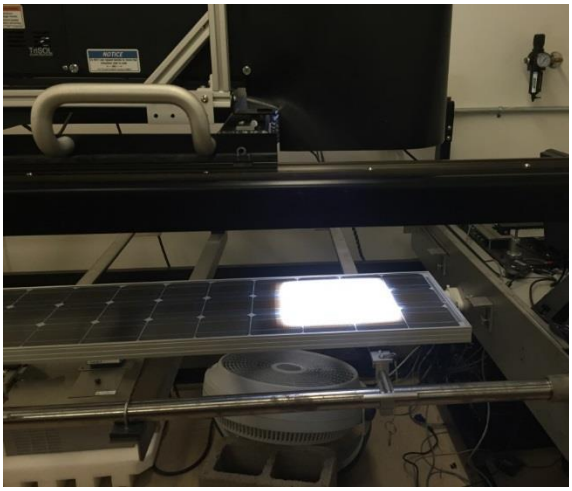

Figure 4: Solar Simulator Beam On the Desired Cell of a Module

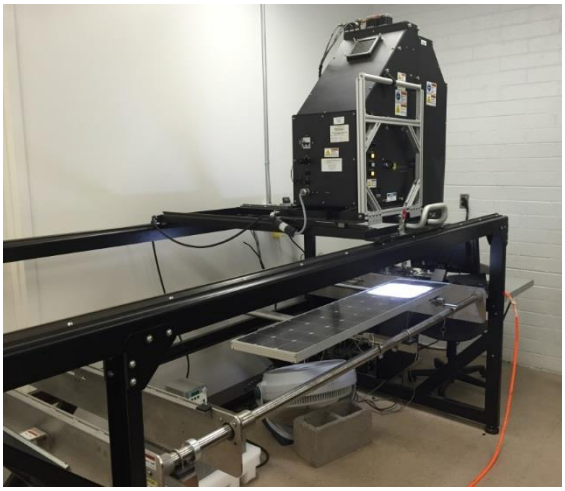

Figure 5: Cell Level I-V Testing Machine for a Module (Solar Simulator)

3.6 Cutting of the PV Module

After the cell level I-V curves are taken for all the cells in a module, their R_{se}, R_{sh} and Fill Factor are analyzed and the best, worst, mean performing cells are selected. After

selection, the cells which are to be cut are marked and are cut using a Dremel tool as shown in the figure. A diamond coated cutting tool is used to cut the cell from the module. The cell after cutting is shown in the figure below. Since the glass is tempered, it tends to break when the cell is cut.

3.7 Cell Extraction

In order to separate the cell from the sample, two methods were developed. The first method was developed using a chemical named trichloroethylene (TCE) and the second method was developed without using the chemical but by using a metal bar and was extracted mechanically. The concept of using trichloroethylene was adapted from Doi et al [18]. This section provides a detailed description about the extraction processes for both the methods in detail.

3.7.1 Extraction of the Cell Using Trichloroethylene

After the cell is cut from the module, in order to separate the glass from the cell, a chemical, trichloroethylene (TCE), is used. This chemical especially is useful in dissolving the encapsulant Ethylene Vinyl Acetate (EVA).

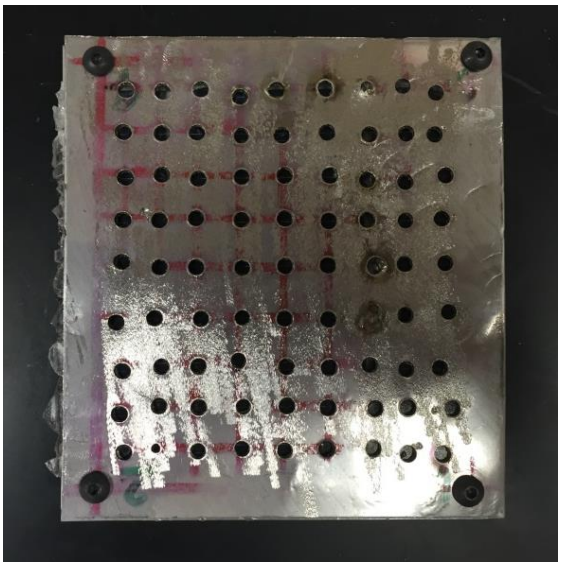

Figure 6: Top View of the Sample

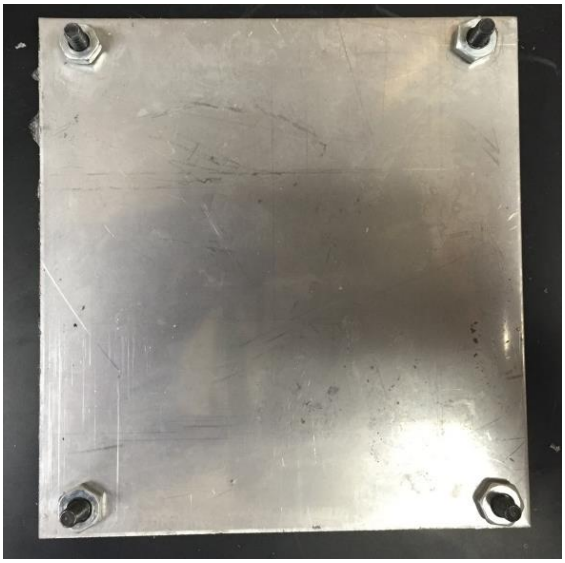

Figure 7: Bottom View of the Sample

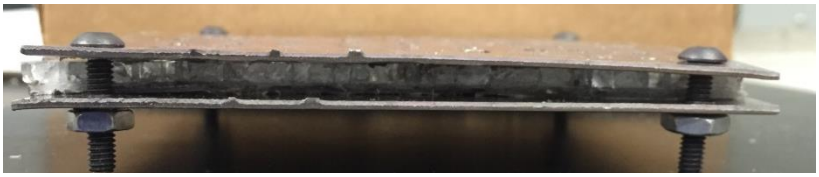

Figure 8: Front View of the Sample

So, in this method, two stainless steel metal plates little larger than the size of the cell are cut and about 1mm-1.5 mm holes were made with uniform distance between them only on the front side of the metal sheet as shown in the figures 6-8. This is done in order to facilitate smooth passage of TCE to the cell through the encapsulant and also the effective removal of the dissolved EVA through the holes. The cell is placed between the two plates and it is immersed in TCE solution. This beaker is then immersed in another beaker filled with water and this apparatus is placed on a hot plate and the temperature is maintained between 50^{o}C – 80^{o}C. This apparatus is left for about 60 -90 minutes and the sample is taken out of the TCE solution and the metal plates are removed. It can be

observed that the glass pieces are separated from EVA and cell, and the cell is separated out. It is to be noted that TCE is a harmful chemical and one must perform all the experiments in fume hood. Figure 9 shows the apparatus used for performing the experiment whereas figures 10 and 11 show the sample cell before EVA dissolution and after dissolution.

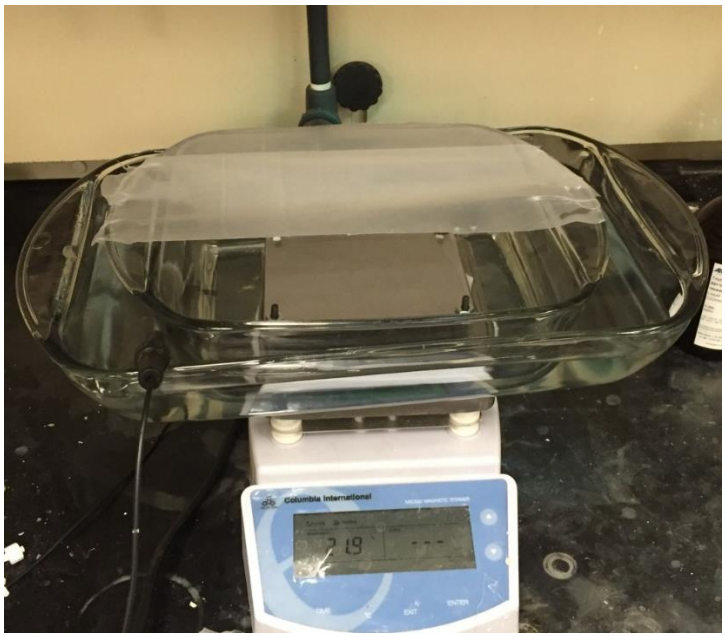

Figure 9: Apparatus for Dissolution of Ethylene Vinyl Acetate

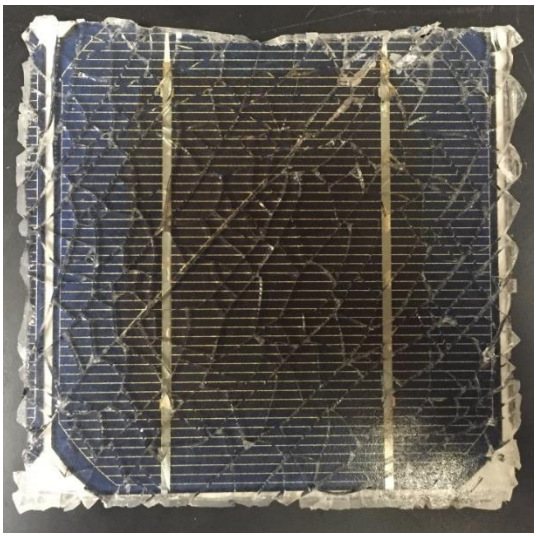

Figure 10: Sample Cell Cut from The Module

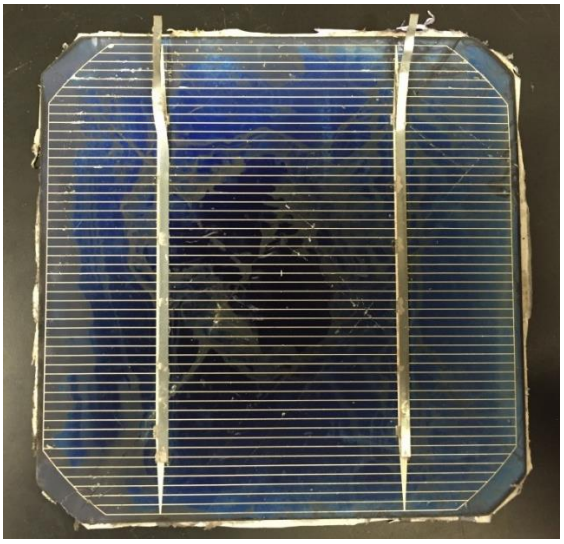

Figure 11: Sample Cell After Removal of Encapsulant

3.7.2 Cell Extraction Using Mechanical Method

Cell extraction using TCE is expected not to have any effect on the solder bond as it is an organic solvent but it needed to be confirmed. In order to confirm this, a mechanical method of removing a strip of the cell from the module without breaking the glass was also utilized. In this method, the backsheet for the desired cell was cut using heavy-duty razor blades and heat gun. Once the backsheet and EVA were removed, the ribbons present on the backside of the cell were also removed. Isopropyl alcohol was then applied on the backside and was polished using sandpaper as shown in the figures 12 and 13.

Figure 12: Isopropyl Alchohol Used for Cleaning

Figure 13: Sandpaper Sheet for Smoothening the Backside of the Cell

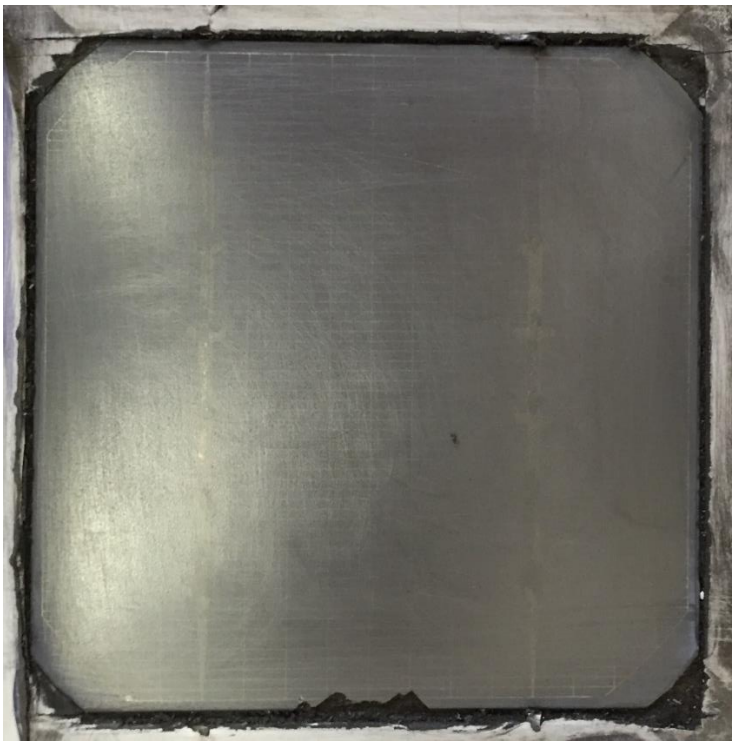

Figure 14: Sample Cell After Smoothening and Removal of Backside Metallization

The sample after backside polishing is shown in figure 14. Once the backside of the cell was polished, a square metal tube was placed on the cell beneath the busbar/ribbon and the cell was cut around the metal tube using a heavy-duty razor blade. 3M epoxy glue DP 460 was used to glue the metal beam to the backside of the cell and it is allowed to set overnight. Figure 15 shows the metal beam before and after the application of epoxy glue and figure 17 shows the setup after the beams were stuck to backside of the cell. Once the glue is hardened and the beam is stuck to the cell firmly, a heat gun was used and heat is provided from the front side of the module over the area of interest. By providing heat for about 5 minutes, the EVA on the front side loosens up and the cell can be extracted from the module as shown in the figure. It is also to be noted that by providing excessive amount of heat, one may melt/affect the solder bond which need to be avoided by

limiting heating time and temperature. This method is a very cost effective method when compared to the TCE method discussed above but a great caution shall be exercised.

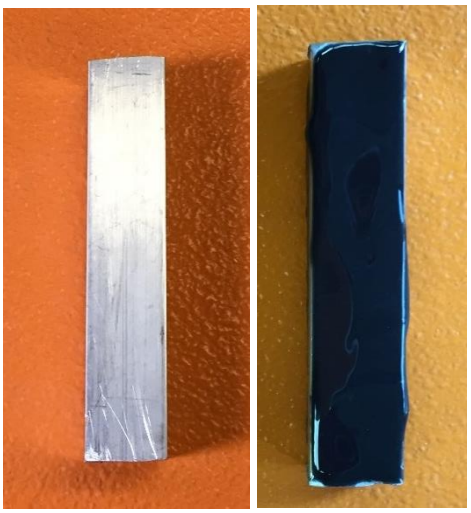

Figure 15: Metal Beam Before and After Applying Epoxy Glue

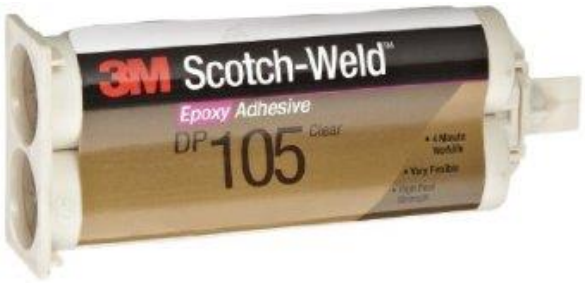

Figure 16: Epoxy Glue Used for Adhesion

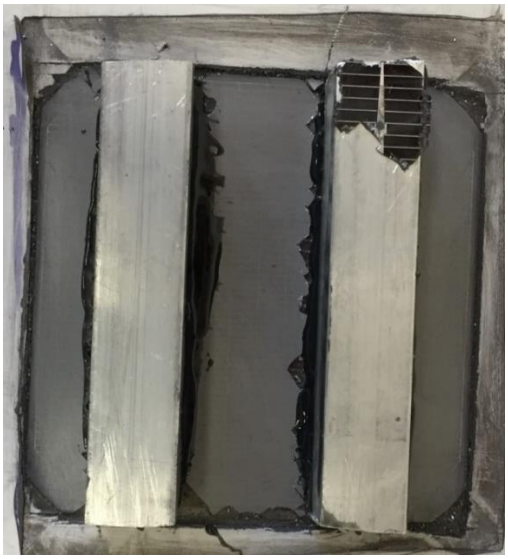

Figure 17: Final Setup After the Beam Is Attached to The Cell Using 3M Epoxy Glue

3.8 Resistance Measurements Using Four-Point Probe Method

Electrical resistivity is a basic material property that quantifies a material's opposition to current flow; it is the reciprocal of conductivity. One of the most common ways of measuring the resistivity of some thin, flat materials, such as semiconductors or conductive coatings, uses a four-point collinear probe. The four-point probe technique involves bringing four equally spaced probes in contact with a material of unknown resistance. A DC current was forced between the outer two probes, and a voltmeter measures the voltage difference between the inner two probes. The resistivity was calculated from geometric factors, the source current, and the voltage measurement. The instrumentation used for this test includes a DC current source, a sensitive voltmeter, and a four-point collinear probe. The figure for the setup of multimeter is shown in figure 18. The four-point probe resistance measurements are done using the SMU 2450 source measurement unit, SP4 - four-point probe head and S-302 test stand. The model set up for the placement of probes over the cell is shown in figure 19.

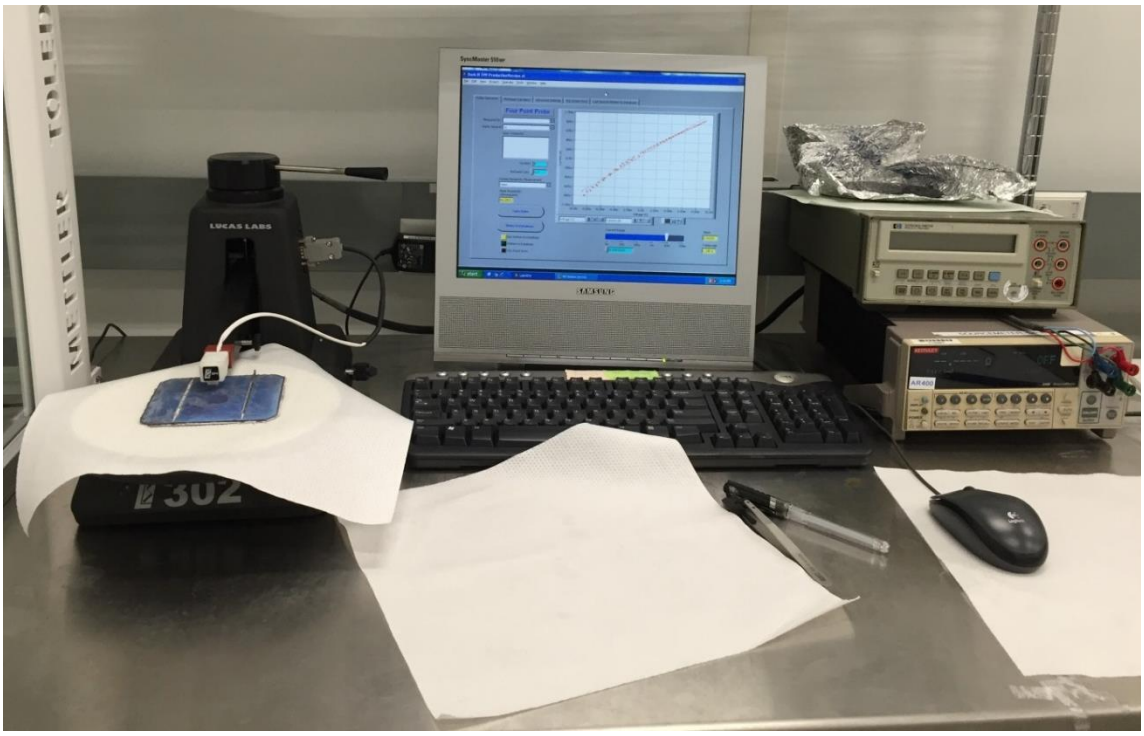

Figure 18: Four-Point Probe Setup Including the Probe and Keithley 2400 Multimeter

Figure 19: Four Probes Touching the Metallization of the Cell

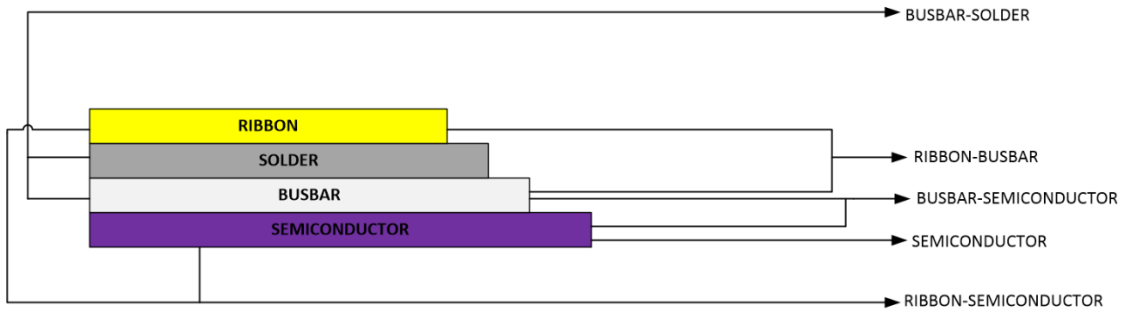

Figure 20: Various Combinations Used for Series Resistance Measurements

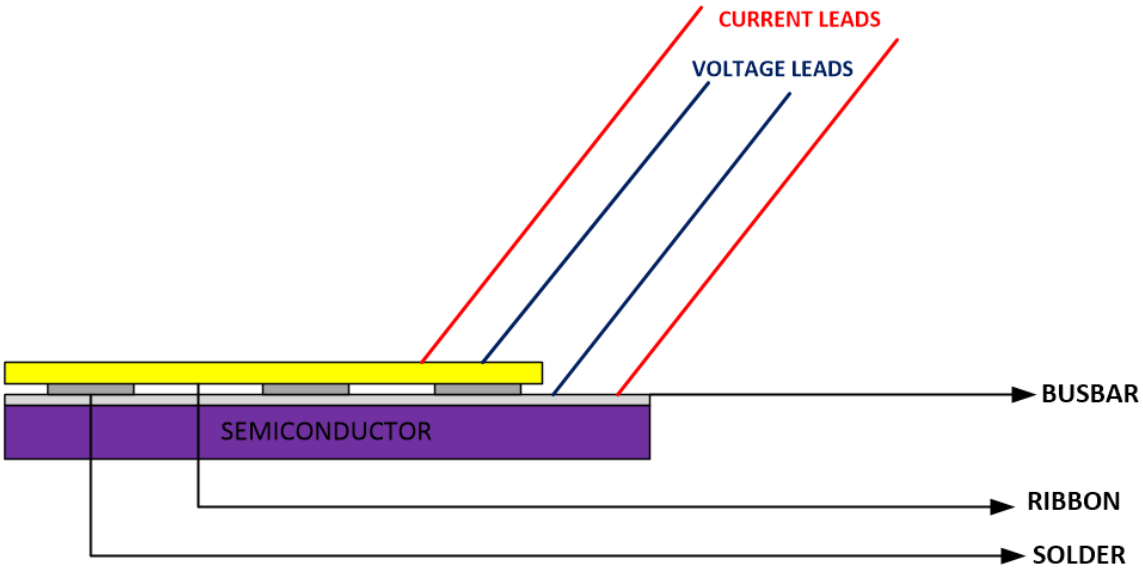

Figure 21: Four-Point Probe Lead Positioning

For the series resistance measurements, all the various combinations possible for causing the resistance were considered. The various combinations used for the resistance measurements are shown in the figure 20. The setup was connected to the multimeter and by using the resistance value shown on the multimeter the series resistance was calculated by using the appropriate formula. For a combination between two surfaces, it

was made sure that two probes were placed on one surface and the other two probes on the other surface as shown in figure 21.

3.9 Climate Specific Thermal Modeling

This section illustrates the methodology that was adapted in calculating the thermal fatigue that was developed in a module when exposed in a particular climate. The thermal fatigue is mainly developed due to two factors. The first factor is the daily temperature change that is the day and night temperatures which effects the solder bond gradually by the expansion and contraction of the solder bond. The second factor is the cloud cycles which occur every day which cause the sudden expansion and contraction in the solder ribbon which might induce cracks in it as the time goes on. In this work, the thermal fatigue for 20 years from 1991 to 2010 in order to have a better understanding of how much fatigue a module can develop over 20 years in different climates.

In order to estimate the fatigue developed, first the weather data was taken from TMY 3 and a program was developed in matlab in order to extract only the data required for the procedure. The total irradiance was calculated using the Liu-Jordan model using matlab software and also by using PVsyst software by converting the meteorological data into PVsyst format. Once the total POA irradiation is calculated, the cell temperature is calculated by using the following formula[15]

$$T_{Cell} = T_{amb} + E.e^{(a+b\,.\,WS)} + E.\frac{\Delta T}{E_o}$$

where a and b were empirically determined for a glass/polymer backsheet module construction deployed in an open-rack configuration to be -3.56 and -0.075, respectively.

E_o is the reference solar irradiance of 1000 W/m2 and ΔT represents the temperature difference between the cell and module at this reference irradiance. For an open-rack configuration ΔT was determined to be 3°C; however, this offset temperature will be sensitive to racking method and module construction.

Once the cell temperature was calculated for every hour, the maximum and minimum temperature difference for a particular day was calculated and also the mean daily maximum temperature was determined. Once these factors were determined, the thermomechanical fatigue is calculated by using the formula[15],

$$D = C.(\Delta T)^n.(r(T))^b.e^{\frac{Q}{k_B.T_{max}}}$$

where ΔT is the mean daily maximum cell temperature change, T_{max} is the mean daily maximum cell temperature, C a scaling constant and Q and k_B are activation energy and Boltzmann's constant. The temperature reversal term, r(T), is the number of times the temperature history increases or decreases across the reversal temperature, T, over the course of a year. The scaling constant C and the reversal temperature T were used to fit this model to our simulated data, while the values of the exponents n and b and the activation energy Q are shared with the Coffin-Manson and Norris-Lanzberg equations for PbSn eutectic solder (C= 240, T= 56°C, n= 1.9, b= 0.33, Q= 0.12 eV). It is to be noted that the scaling constant C and the reversal temperature T values are valid only for a 1-minute data intervals. The reversal temperatures and scaling constants for various time intervals are given in the following table [15].

Table 1: Scaling Constants and Reversal Temperatures for Various Time Intervals

Time Interval (min)	C	Reversal Temperature
1	239.9	56.4
5	249.9	56.9
30	344.1	55.8
60	405.6	54.8

For this work, a time interval of 60 mins were used and hence a scaling constant of 405.6 and a reversal temperature of 54.8^{o}C was used. This process was repeated for every year for 20 years and the cumulative fatigue was calculated for all the four sites.

4.0 RESULTS AND DISCUSSION

Results from module characterization, cell extraction, cell characterization and climate specific thermal modeling are discussed in this chapter below. For the experiments, 6 modules from three different climates were used. There are a total of three modules from Arizona which are from a hot and dry climate, two modules from California which are from a temperate climate and one module from Mexico which is from a warm and humid climate. The classification of modules and the tests performed are shown in the following flow chart.

4.1 Module Characterization:

4.1.1 Cell Level Dark I-V curves:

In this sections, all the tests performed before the destruction of the modules are discussed. All the modules were cut on the back side of each cell and were soldered using the soldering gun and ribbon as described in the methodology. These soldered modules are connected to the solar simulator machine one after the other in order to perform cell level dark I-V curve tests. A sample report from the dark I-V curve is shown in the following figure.

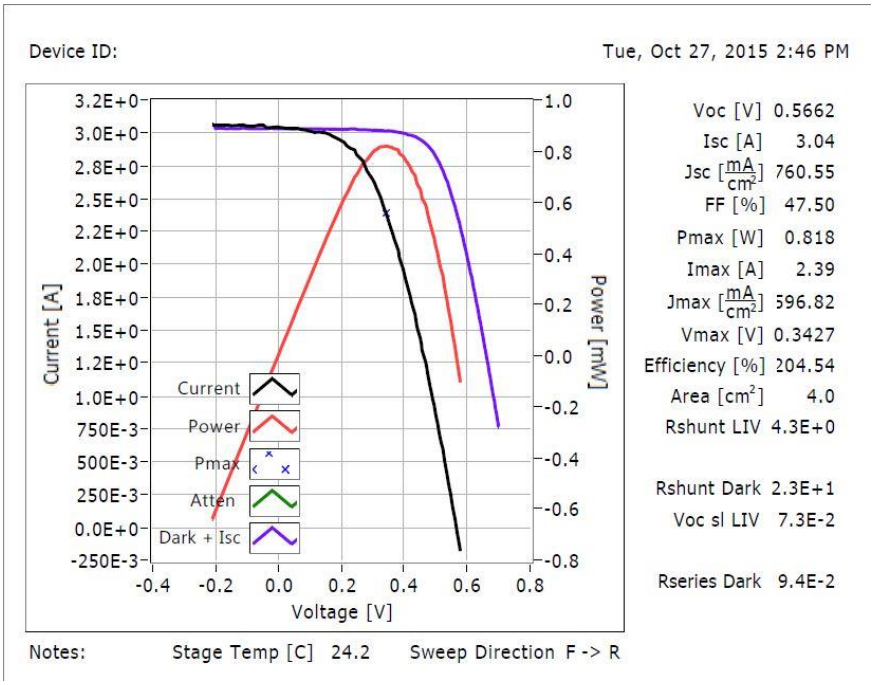

Figure 22: Sample Report Generated for I-V Curve from Indoor Solar Simulator

The following graph shows the relationship between the series resistance and fill factor for all the modules at cell level. From the graph we can observe that the fill factor of the cell decreases with the increase in series resistance. The highest drop in the fill factor is observed for the cells from Mexico module (P29005) due to their high series resistance. The high series resistance is observed due to their high field exposure (23 years) and also due to the climate in which they were exposed (warm and humid). Due to the humid conditions, the moisture ingresses through the backsheet of the modules and creeps into the solder joints causing corrosion which depletes the ribbon contact with the busbar. When this happens, the electrons generated in the cell have to find an alternate but a narrow and long route in order to get transferred from cell to ribbon thus increasing the series resistance. After Mexico module, the worst series resistance is shown by the Arizona field exposed module (514210) which is exposed for 18 years in hot and dry

climate. The other exposed module from Arizona (464185) shows series resistance values very close to that of the control module which indicates that the solder bonds in the modules are practically intact and show very less degradation. The California aged module shows higher series resistance when compared to the California control module as expected. California module are expected to have lower series resistance than Arizona modules due to their temperate climate and also due to lesser cloud cycles.

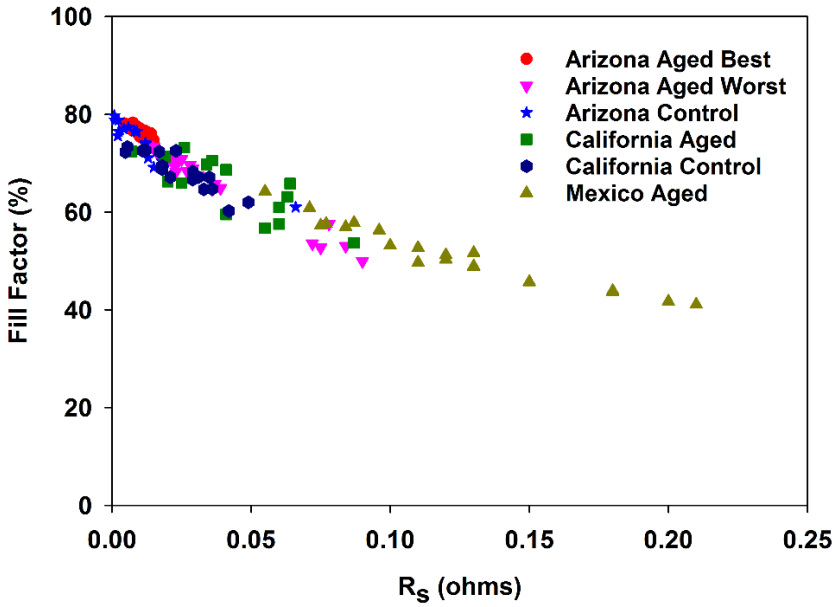

Figure 23: R_S Vs FF for Modules from Different Climates at Cell Level

The relationship between the shunt resistance (R_{SH}) and Fill Factor is shown in figure 24. The values for R_{SH} were also obtained from the cell level dark I-V curves. It can be observed that the fill factor of the cell increases with increase in shunt resistance which is expected. High shunt resistance implies lower defects in the cell which indicates a better performance. When the trends in the previous figure are combined with this figure, it can be see that R_S plays the primary role and Rsh plays an insignificant role in FF reduction.

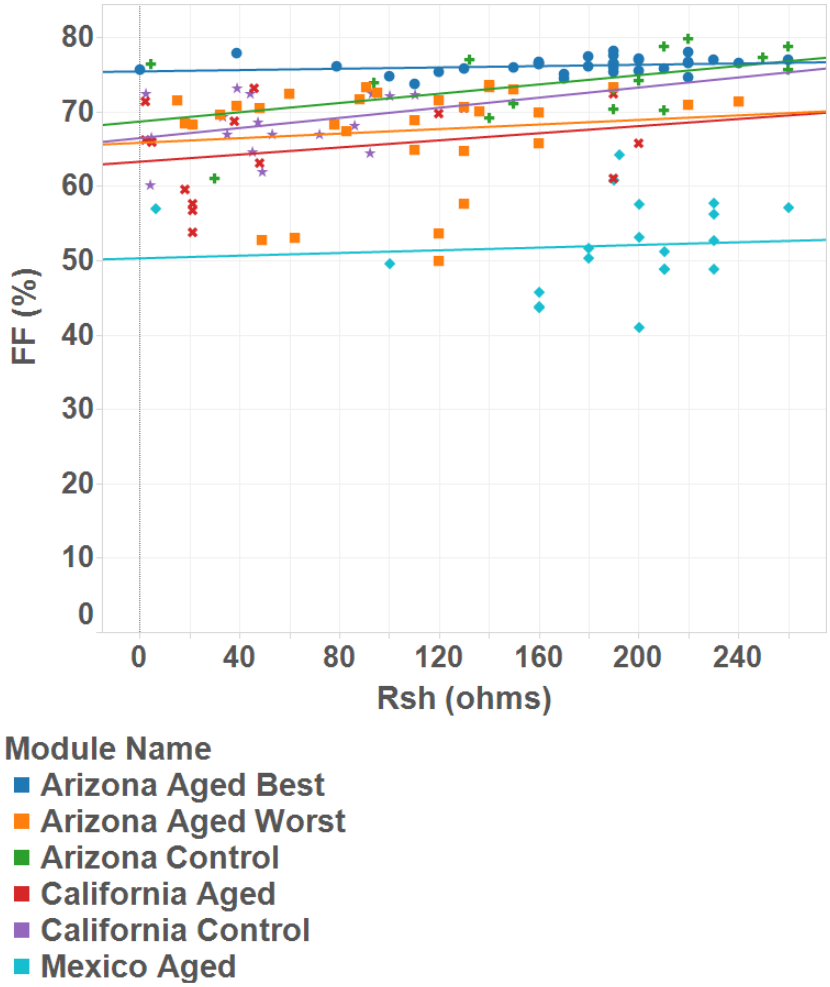

Figure 24: R_{SH} Vs FF for Modules from Different Climates at Cell Level

The box plot for the trend in Fill Factor and Series resistance is shown in figure 25. As seen from the figure, it can be clearly seen that as the series resistance increases, the fill factor decreases.

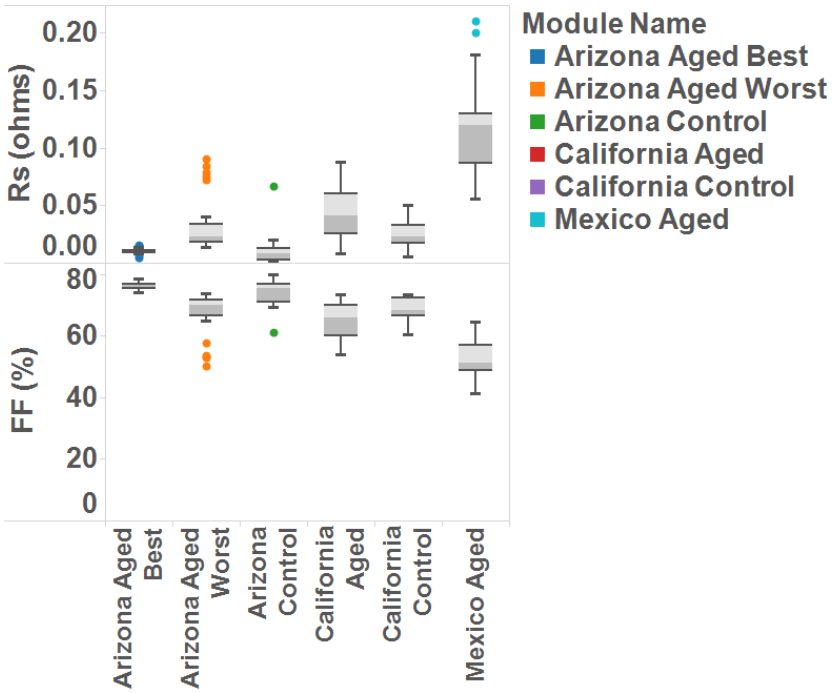

Figure 25: Box Plots for R_S and FF for Modules from Different Climates

4.1.2 Effect of Temperature On Characteristic Resistances of a Module

In this section, the effect of temperature on the series and shunt resistance in a module is described. One module from Arizona (aged, 464185) and one module from Mexico (aged, P29005) were used for the experiments. The I_{SC} current was passed through each cell in the dark and the IR image was taken using FLUKE IR camera. After the image was taken, the temperatures at the center, edge and ribbons of each cell were taken and compared against the dark I-V series and shunt resistance of each individual cell. Figures 26 and 27 show the effect of temperature on the series and shunt resistance for the Mexico (P29005) module.

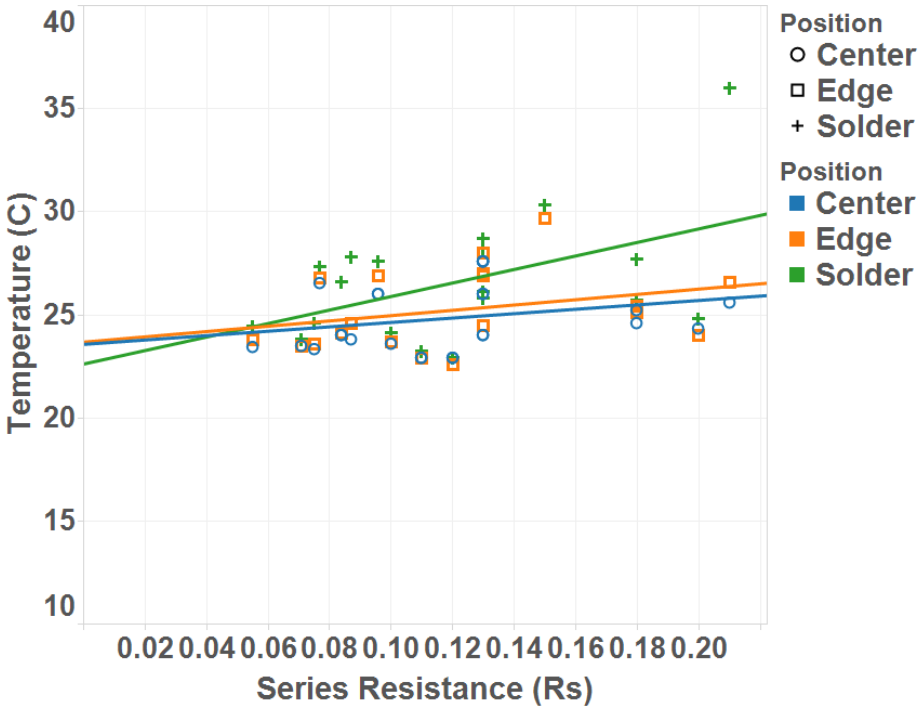

Figure 26: Series Resistance Vs Temperature for Mexico Module

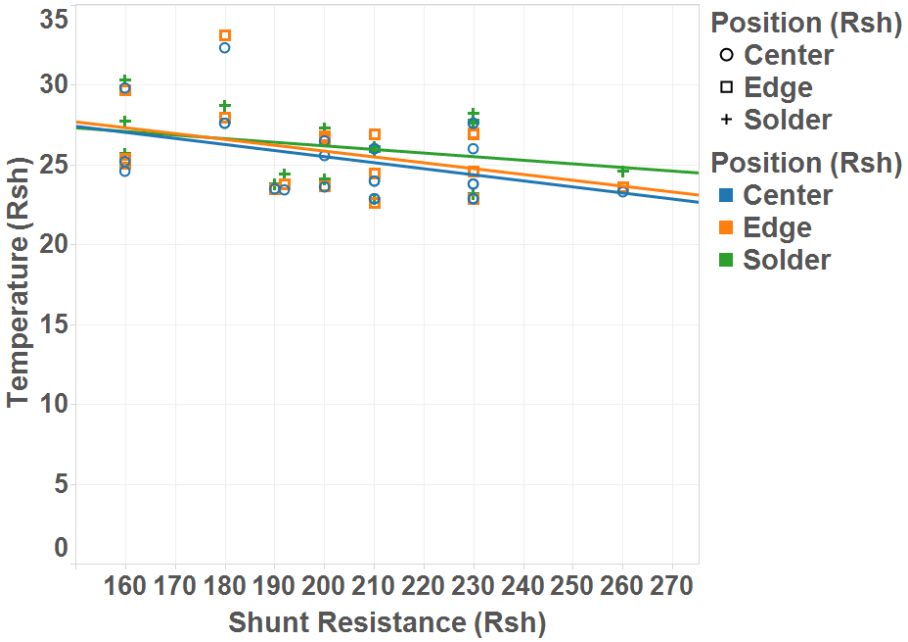

Figure 27: Shunt Resistance Vs Temperature for Mexico Aged Module

From the above figures, it can be observed that the temperature is directly proportional to the series resistance. When the temperatures at three different position of a cell are considered, the temperature at the ribbon of the cell is higher when compared to the temperatures at the center and edge of the cell respectively.

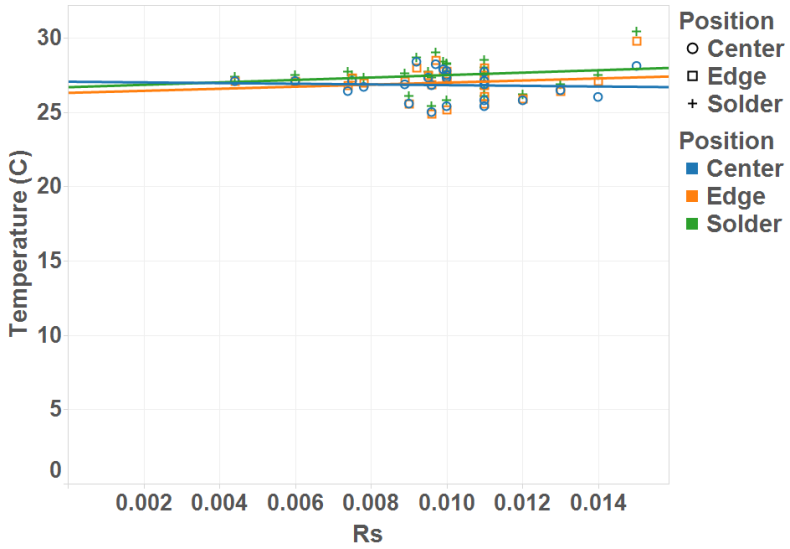

Figure 28: Series Resistance Vs Temperature for Arizona Aged Module

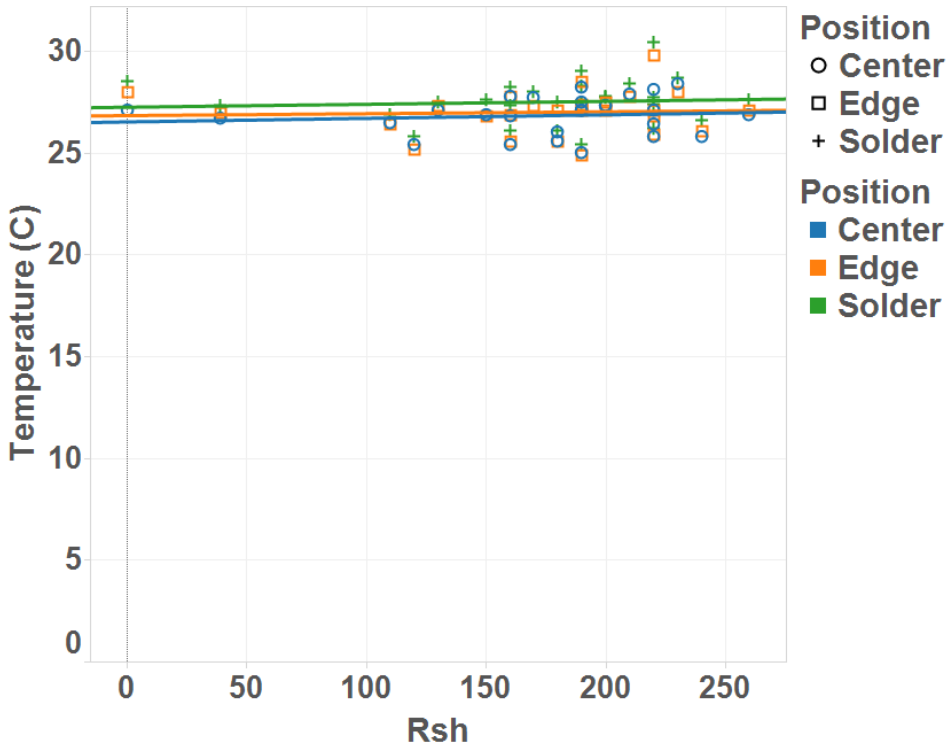

Figure 29: Shunt resistance vs Temperature for Arizona aged module

The above figures 28 and 29 show the effect of temperature on the series and shunt resistances of an 18-year-old Arizona module (464185). It can be observed that the temperature has an increasing trend with increase in series resistance. But when compared to that of Mexico aged module, the rate of increase in temperature is less in the Arizona module because the values of cell level series resistance from dark I-V curves are lower when compared to that of Mexico aged module. For the Arizona aged module, the temperature almost seems to remain constant with increase in the series resistance and also remains almost the same for all the three different locations in the cell.

4.2 Cell Extraction

In this section, the results of the removal of Ethylene Vinyl Acetate (EVA) by using trichloroethylene are presented. In order to understand the degradation of solder bonds in PV modules, it is very important to separate the solar cell from the EVA and the glass without the solder bond getting damaged. After a detailed literature review, it was understood that trichloroethylene (TCE) was believed to perform this job much better than other chemicals. Hence it has been decided to perform the further experiments using this chemical.

The initial set up for the experiment is shown in figure 30. As seen in the figure, the sample is supported by a glass sheet on the back and are bound by binder clips in order to provide necessary clamping force to prevent swelling when in TCE solution. The set up for the apparatus is shown in figure 31. As seen in the figure, the sample setup is put in a beaker and the TCE solution is filled until the sample is completely immersed and this beaker is placed in a larger beaker filled with water and this is put on a water heater with a stirrer.

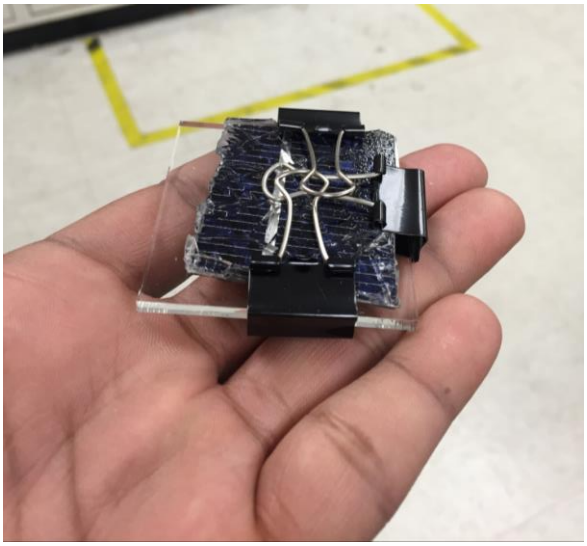

Figure 30: Initial Sample Setup

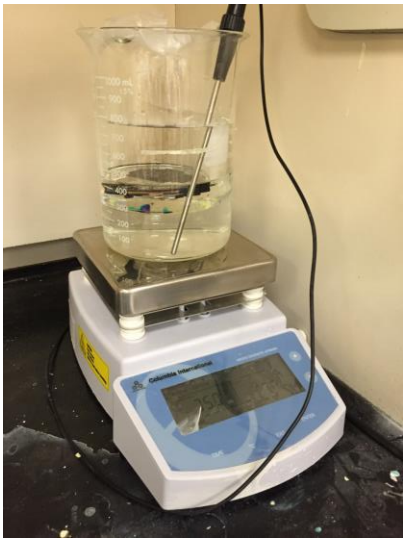

Figure 31: Initial Apparatus Setup

This apparatus was left untouched for a day and then it was removed and it was analyzed. The cut module after the experiment is shown in figure 30. It was observed that:

1. The cracked glass separated from the cell.
2. The glass backing was separated from the cell. (The clips were attached to the edge of the cell hence they might have come off once the EVA started to swell)
3. The back sheet crippled as shown in the figure 32.

Figure 32: Sample After the Experiment

After analyzing the result, it was concluded that the following might be the possibilities that would have triggered this result.

1. The clips attached might come off making the back part to cripple.
2. May be 100% TCE is not recommended.
3. Cracked glass might be the problem.

Hence by keeping these issues into consideration, in the next experiment, two glass sheets and larger binder clips were used in order to provide more binding force and to keep the glass intact. The set up was placed in 100% TCE solution and was placed in the apparatus as described above. Again, the sample was left for a day. The observations after the removal of sample from the set up are shown in figures 33-34. From the below figures, it can be observed that,

1. EVA and Glass were completely separated on the edges on all 4 sides.

2. TCE did not reach the middle of the sample, hence glass and EVA were not separated.

3. Clamping force was adequate, hence the back sheet of the obtained sample stayed intact.

From these results it can be observed that there was an improvement in the setup but there was no removal of the EVA in the middle of sample.

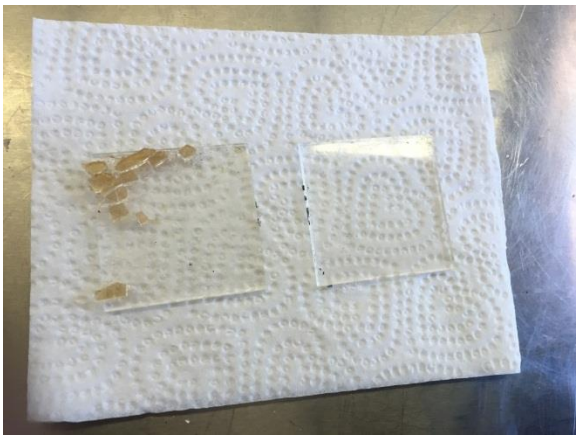

Figure 33: Front and Back Side of the Glass

Figure 34: Removed Sample from TCE Solution

In the next process, a sterner and stronger set up was used so that TCE reaches the center of the sample. In this set up, two stainless steel plates of around 1.5 mm thickness were cut and holes were drilled and were clamped using nuts and bolts as shown in figures 35-37. This set up was immersed in 100% TCE solution and was left for a day at 80^{o}C.

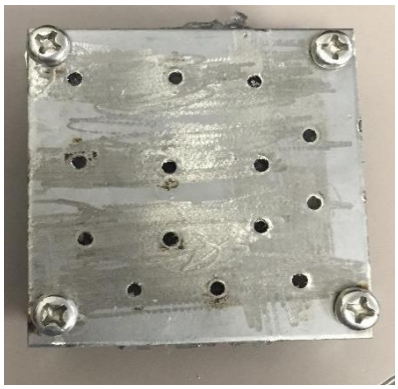

Figure 35: Top View of the Mini Setup

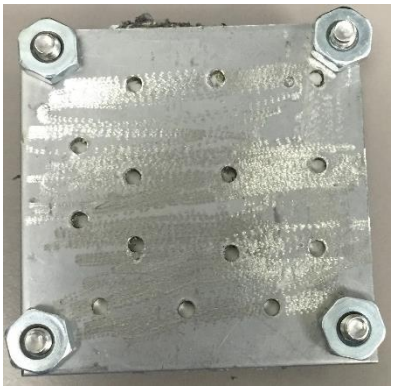

Figure 36: Bottom View of the Mini Setup

Figure 37: Front View of the Mini Setup

After a day, when removed, it was observed that all the TCE was evaporated and when the set up was unclamped it was observed that all of the EVA was dissolved and the cell and the back sheet were completely separated from one another as shown in figure 38.

Figure 38: Separated Backsheet and Cell After Experiment

In the first 3 experiments we observed that all the TCE was evaporated when the temperature of water raises to 80^{o}C. Since we are looking to perform peel test on solder bonds it is better to have the EVA between the cell and back sheet intact as it holds the cell much better during the test. Hence we decided to observe the TCE dissolution process for every hour in order understand the dissolution process much better and save TCE since it's a very costly chemical.

In the final experiment, the hourly EVA dissolution process was observed. The setup, the apparatus and all the procedure for the experiment remained the same. The set up was placed in TCE solution and the experiment was started at 10.05 am. The sample was

removed from the TCE solution at 11.05 am and the set up was unclamped and the sample was observed. It was observed that all the glass and the EVA was completely separated from the cell and the EVA between the cell and the back sheet remained intact. And after 2 more hours, it was observed that, the EVA between the back sheet and the cell also dissolved. The cell after the first hour is shown in figure 39.

Figure 39: Sample After One Hour in TCE Solution

Hence it can be inferred that, since stainless steel is a far better conductor than glass, the process takes place at a faster rate than usual hence completing the dissolution in an hour. This is a very useful observation and saves a lot of time.

As this process has been finalized, a new stainless steel setup was built as described in the methodology section which could accommodate the size of a regular PV cell. The following figure shows the time taken for extraction of the cell that is the time taken for

the dissolution of Ethyl Vinyl Acetate (EVA, encapsulant) for different modules from different climatic conditions is shown in figure 40.

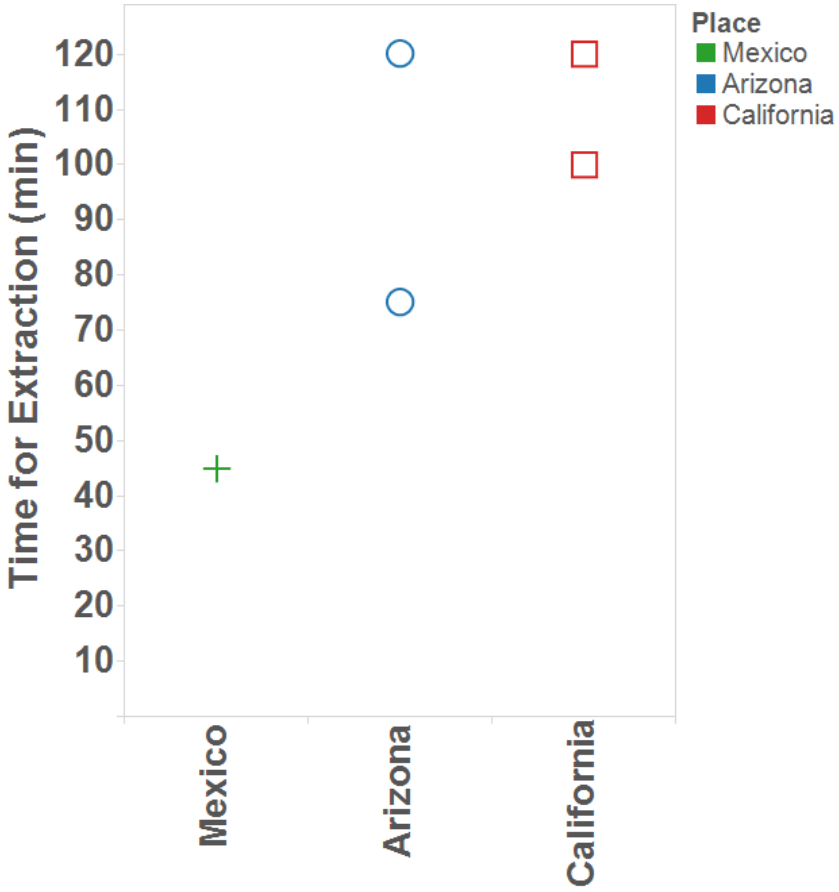

Figure 40: Time Consumed for The Dissolution of EVA for Various Samples

From the above figure, it can be observed that the Mexico aged module requires the least amount of time for the dissolution of EVA followed by Arizona aged and California aged. Both the control modules from Arizona and California require the maximum amount of time for the dissolution process to complete. The variation in time is due to the weakened interfaces between the Glass/EVA and Cell/EVA. This might be caused due to various factors such as the amount of UV radiation incident, ambient temperature and

also the relative humidity. The following table shows the various factors which can aide the weakening of the interface and compares them against different climates.

Table 2: Factors Affecting the Dissolution of EVA

	Arizona	California	Mexico
Relative Humidity (%)	33.4	67.3	53.6
Average Annual Maximum Temperature (^oC)	38	23.1	32.9
Total UV radiation (kWh/m^2)	4.925	7.038	6.197
Age of the module (years)	18	28	23

The interface is most weakened when the module is placed in Mexico due to its humid nature. The moisture ingression over the years weakened the interface thus allowing moisture to pass to the cell thus causing corrosion which can be see via Fill Factor drop and increased series resistance. Arizona has the next weakest interface when compared to California. This might be due to the thermal cycling which happens over the years. The continual expansion and contraction due to the sudden changes in temperature over the years weakens the interface gradually hence the easier removal of EVA.

4.3 Comparison of Cell Extraction Methods

As described in the methodology, two methods were developed in order to extract the cell from the sample piece removed from the module. The following table compares the characteristics of both the methods.

Table 3: Comparison of Different Methods Used for Cell Extraction

Factor ↓	Chemical Method	Mechanical Method
Time	1-2 hours	8-10 hours
Sample Size	size of a single cell	A strip of cell along solder
Hazardous	Very hazardous	Not hazardous
Cost (for 5 samples)	$60	$35

Table 2 gives a good understanding of various factors involved in each method. The chemical method is a fast method for dissolution of EVA using trichloroethylene solution but this procedure has to be performed very carefully inside the fume hood as trichloroethylene is a very dangerous chemical and experiments performed using TCE must be done using personal protective equipment. On the other hand, the mechanical method is very safe method which can be performed without fumehood.The drawbacks with this method are time consumed and the size of the sample that can be extracted. But the most recommended way is that if there is a need for extraction of a complete cell, the chemical method under proper supervision can be used.

The mechanical method is recommended for samples of shorter size and this method is very effective as the samples can be prepared overnight and removed in the morning.

4.4 Cell Characterization

This section deals with the characterization methods applied to the cells which were extracted using both chemical and mechanical methods. The main characterization method used was the peel test. Figure 41 shows the peel strength between the ribbon/busbar interface for different cells in Arizona aged modules.

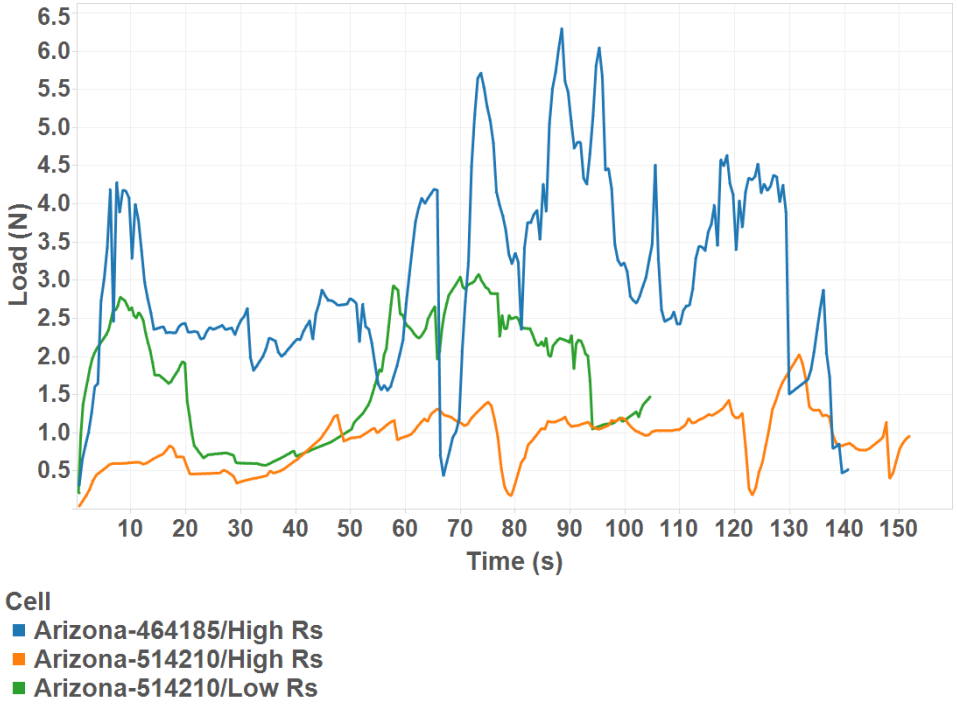

Figure 41: Peel Strength Between Ribbon/Busbar Interface for Cells in Arizona Aged Modules

In the above figure, peel strength plot was plotted for cells extracted using the chemical method mentioned above. From the field aged Arizona module 514210, the cells with highest R_S and lowest R_S were used for the peel test whereas from the field aged Arizona module 464185, the cell with the highest R_S was used. When a cell has high series resistance, the peel strength is supposed to be low. This graph shows the peel strength of

514210 has a lower peel strength when compared to 464185. This is due to the higher series resistance of 514210 cells when compared to those of 464185.

Figure 42 shows the Peel Strength comparison of cells in Arizona aged module using different extraction methods. This graph shows the peel strength for 2 cells of same R_S for two different methods from Arizona aged module (464185). As we can see from the graph, except from a small portion of time (70 to 90 seconds), the mechanical method has a lower peel strength which may be because of the improper soldering of ribbon to the bus bar while manufacturing.

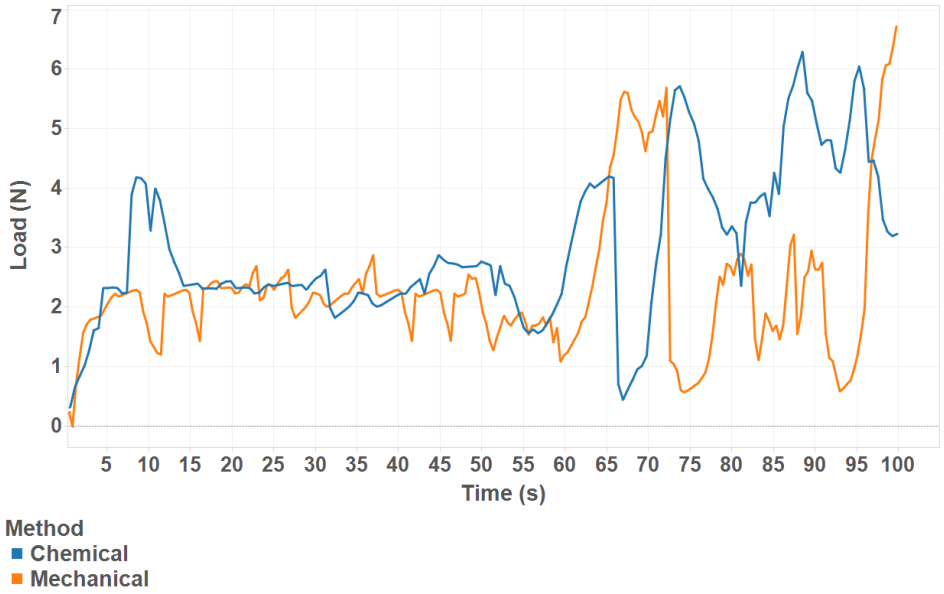

Figure 42: Peel Strength Comparison of Cells in Arizona Aged Module Using Different Methods

Figure 43 shows the peel strength between the ribbon/busbar interface for different cells in Mexico aged modules. Three cells from the Mexico module with High, Average, and Low R_S were extracted and peel test experiments have been performed on them. From the figure, it can be seen that the cell with the highest series resistance has the lowest peel

strength followed by the cells with average and high series resistance. The high series resistance is due to the weak interface between the ribbon and the busbar. This happens mainly due to the continuous thermal fatigue accumulated throughout the years of exposure or due to the corrosion of solder joints due to moisture ingression or due to the improper soldering at the time of manufacturing.

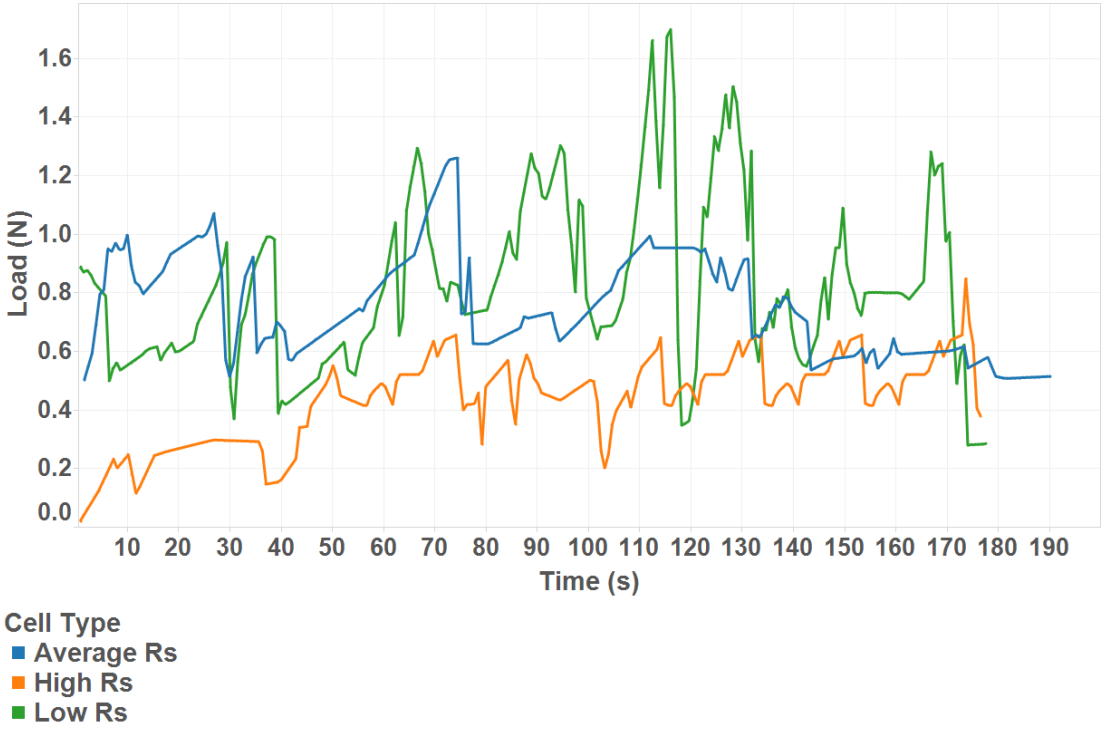

Figure 43: Peel Strength Between Ribbon/Busbar Interface for Cells in Mexico Aged Modules

Figure 44 shows the Peel Strength comparison of cells in Mexico aged module using different extraction methods.

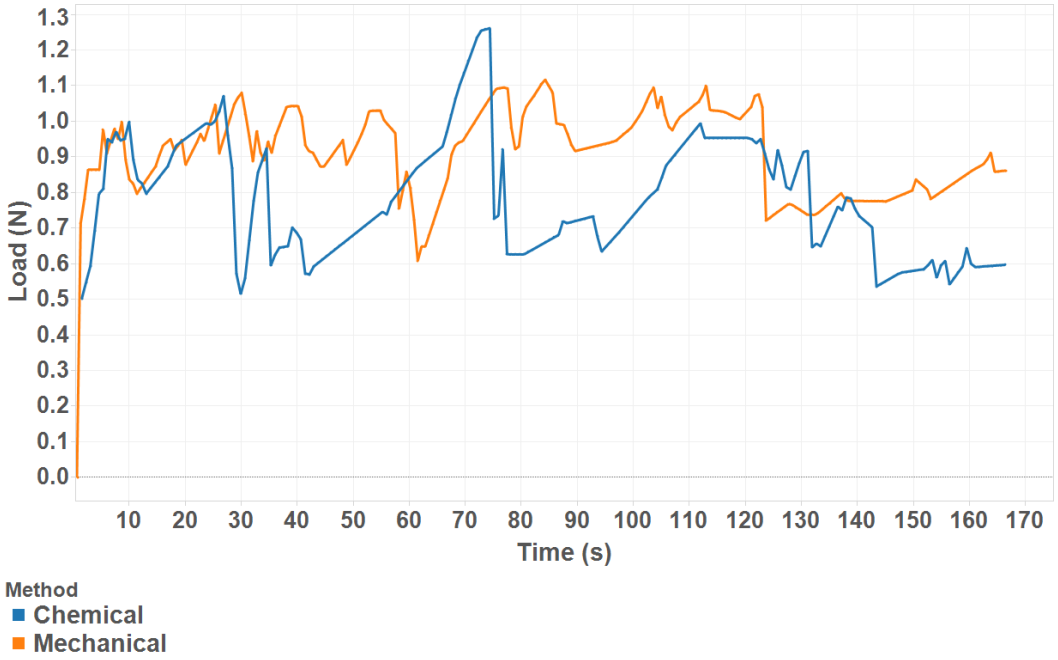

Figure 44: Peel Strength Comparison of Cells in Mexico Aged Module Using Different Methods

Unlike the Arizona aged module, the cells for which the peel tests experiments were conducted for the above graph did not have similar series resistance. The chemically extracted cell had a little higher series resistance when compared to the mechanically extracted cell. Hence we can observe lower peel strength for the chemically extracted cell. The average load required to peel the ribbon for the mechanical method was 0.91N whereas it was 0.79N for the mechanical method.

Figure 45 shows the peel strength comparison between cells from Arizona aged and Mexico aged modules. In this figure, the peel strength of the cell with highest series resistance from each module was compared. From the figure it can be observed that the peel strength decreases with series resistance. Cell from Mexico aged module has the

highest series resistance thus experiences the lowest peel strength followed by Arizona aged modules 514210 and 464185.

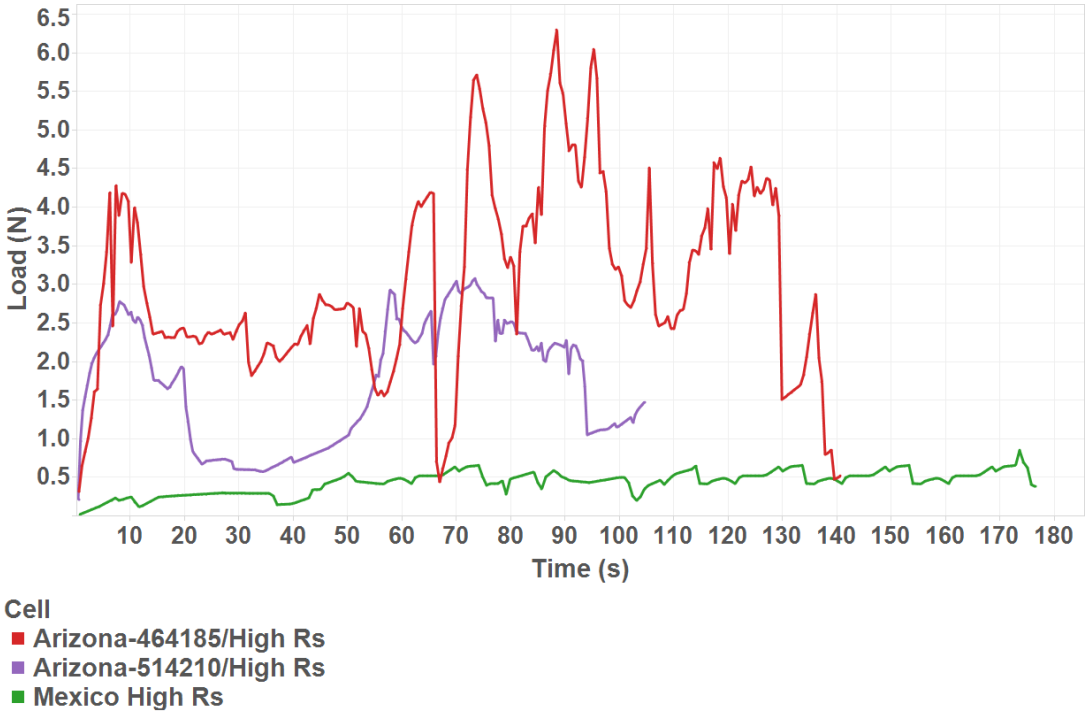

Figure 45: Peel Strength Comparison Between Cells from Arizona Aged and Mexico Aged Modules

Figure 46 shows the combined plot for peel strength of cells from various modules. It can be clearly seen that the highest peel strength is observed for the cells with the lowest series resistance.

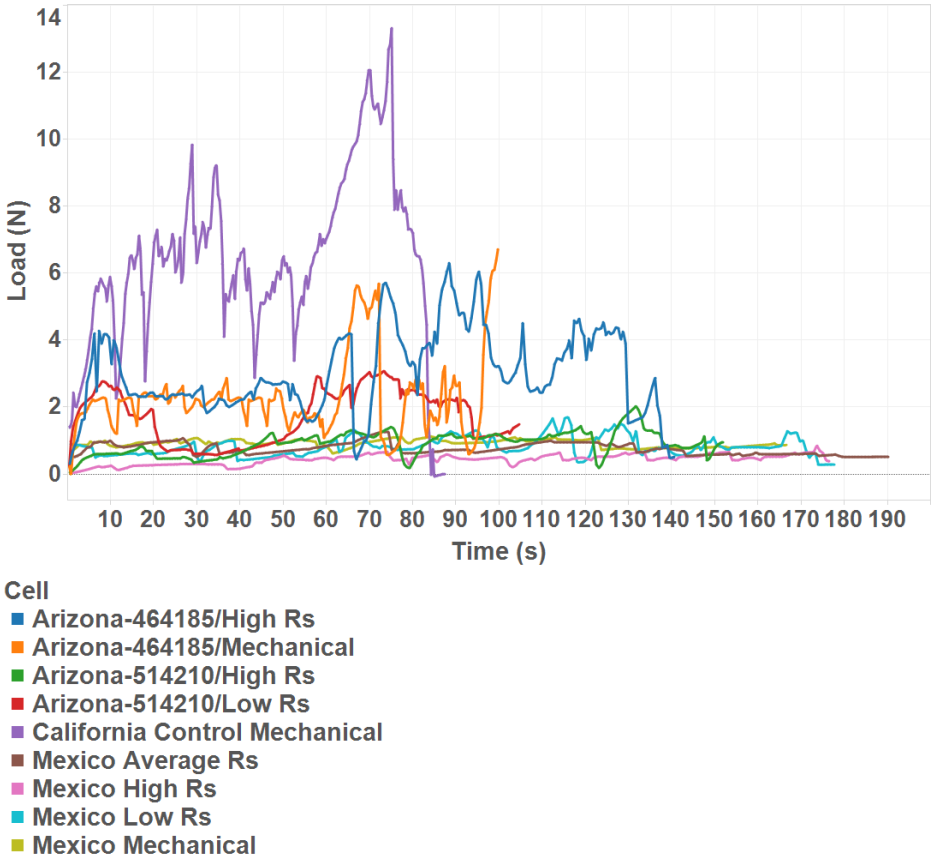

Figure 46: Comparison of Peel Strength for Cells from All Modules

4.5 Four Point Probe Resistance Measurements

This section deals with the four-point probe resistance measurements in order to understand the resistance offered by different combinations between solder, ribbon, busbar and fingers (metallization). The samples used for four-point probe resistance measurements were extracted from Arizona aged/control and Mexico aged modules. It is to be noted that in this section, for all the resistance measurements the trend followed and its relationship with the Fill Factor is only being observed.

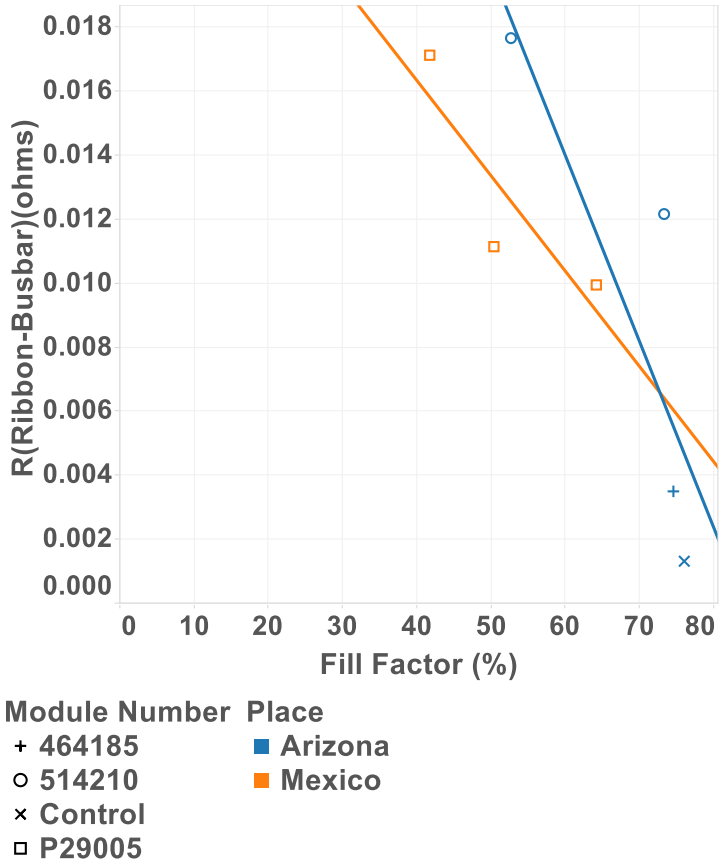

Figure 47: $R_{(Ribbon- Busbar)}$ Vs Fill Factor of Cells from Arizona and Mexico Aged Modules

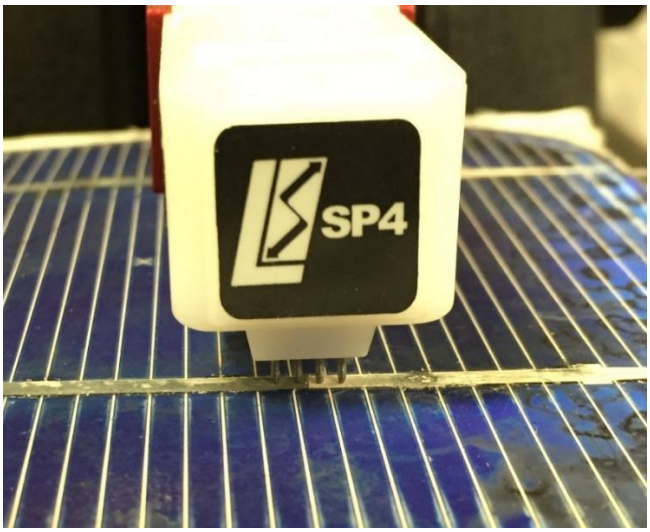

Figure 48: Placement of Four-Point Probe for Ribbon-Busbar Measurement

Figure 47 shows the variation of $R_{(Ribbon- Busbar)}$ with Fill Factor for cells from Arizona field aged/control and Mexico field aged modules. From the graph below, it can be observed that a decreasing trend is seen in FF with increasing resistance. This combination of resistance has the highest values of series resistance when compared to other busbar combinations. In this graph, a higher rate of decrease in Fill Factor can be seen in Arizona modules than the Mexico module. The placement of the probes for the ribbon-busbar combination is shown in figure 48.

Figure 49 shows the variation of $R_{(Busbar - Fingers)}$ with the Fill Factor for cells from Arizona field aged and Mexico field aged modules. This resistance was obtained by placing two probes on the busbar and the other two probes on the fingers of the cell. From the graph, it can be observed that the Fill Factor of the Arizona aged module doesn't get affected with the increase in resistance whereas for Mexico aged module, a decreasing trend in Fill Factor is observed with increase in in the resistance between busbar and fingers.

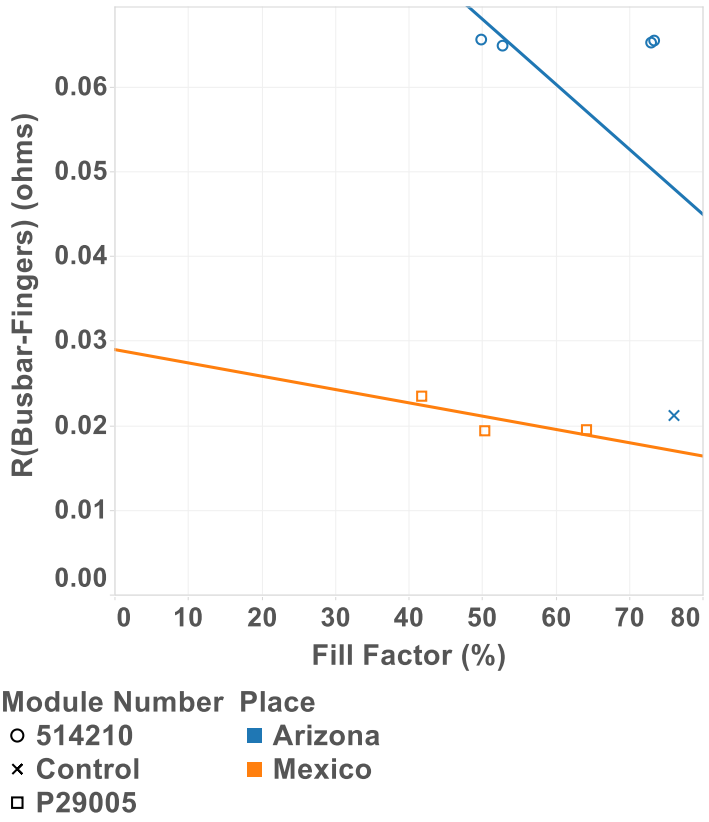

Figure 49: R $_{(Busbar - Fingers)}$ Vs Fill Factor of Cells from Arizona and Mexico Aged Modules

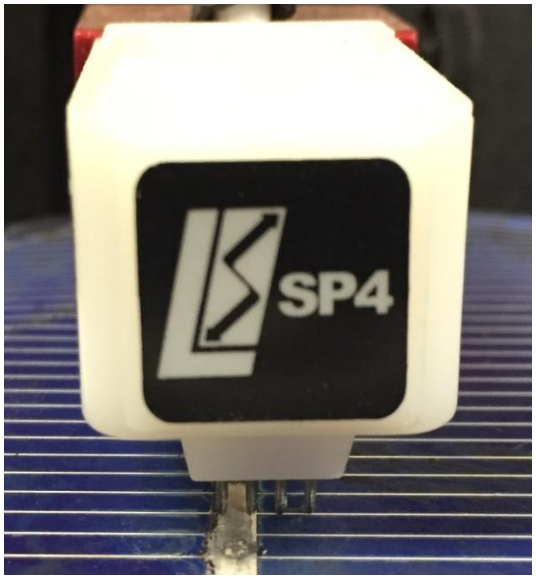

Figure 50: Placement of Four-Point Probe for Busbar-Fingers Resistance Measurement

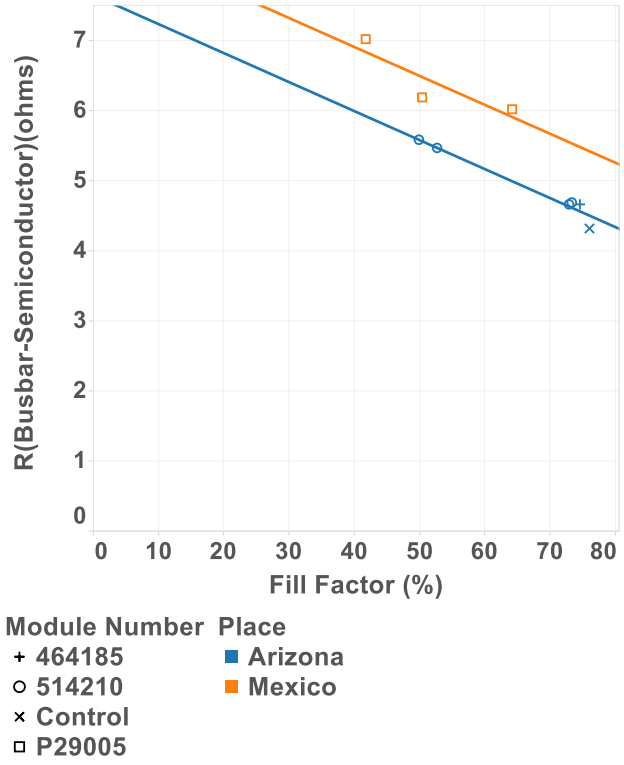

Figure 51: R (Busbar - Semiconductor) Vs Fill Factor of Cells from Arizona and Mexico Aged Modules

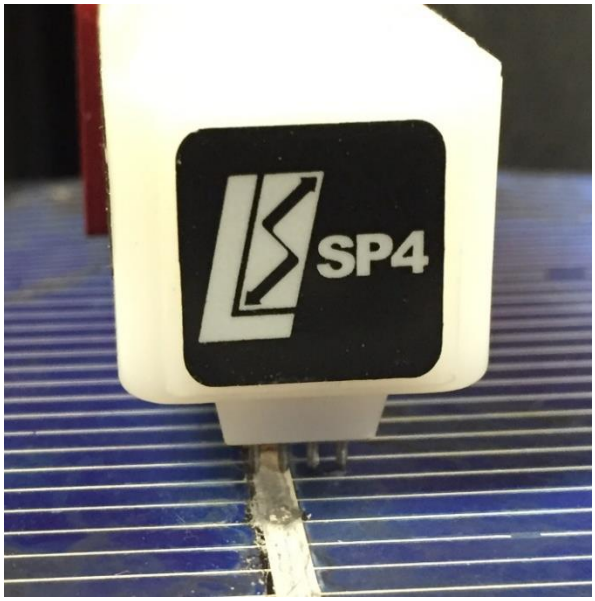

Figure 52: Placement of Four-Point Probe for Busbar-Semiconductor Resistance Measurement

Figure 51 shows the variation of $R_{(Busbar - Semiconductor)}$ with Fill Factor for cells from Arizona and Mexico aged modules. From the figure it can be observed that both Arizona and Mexico aged modules show a decreasing trend in Fill Factor with increase in resistance. Also from the graph, it can be observed that the rate of decrease in Fill Factor is almost the same for Arizona and Mexico aged modules.

Figure 53 shows the variation of $R_{(Busbar - Solder)}$ with Fill Factor for cells from Arizona and Mexico aged modules. From the figure it can be observed that both Arizona and Mexico aged modules show a decreasing trend in fill factor with increase in resistance. Also from the graph, it can be observed that the resistance values for these samples are almost same to those of $R_{(Busbar - Ribbon)}$. The relationship between these resistances van be given by

$$R_{(Busbar - Ribbon)} = R_{(Busbar - Solder)} + R_{(Ribbon)}$$

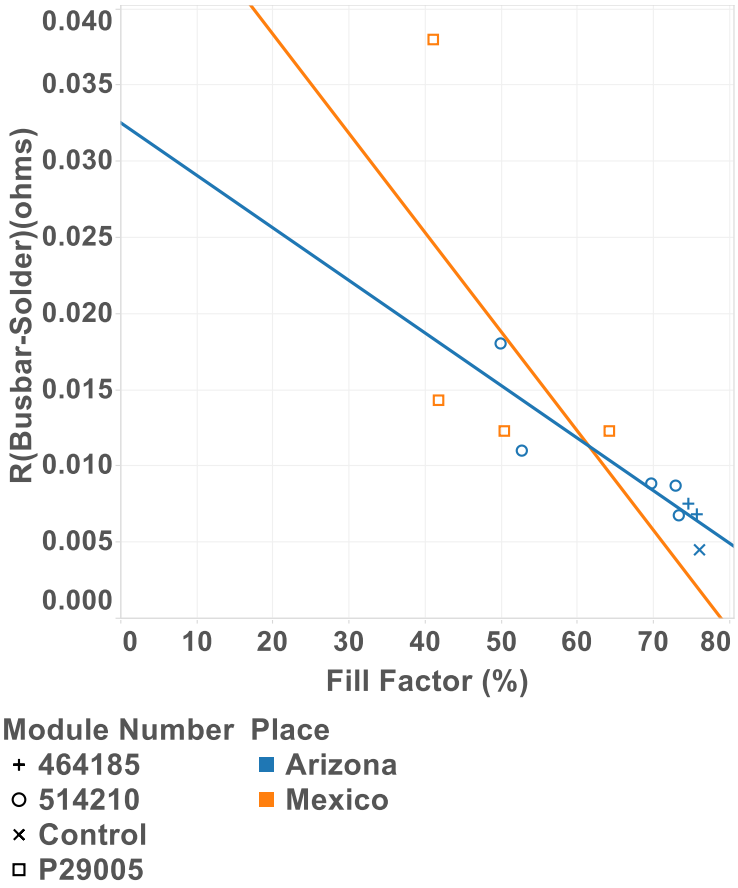

Figure 53: R $_{(Busbar - Solder)}$ Vs Fill Factor of Cells from Arizona and Mexico Aged Modules

Figure 54: Placement of Four-Point Probe for Busbar-Solder Resistance Measurement

Figures 55 and 57 show the variation of $R_{(Ribbon - Semiconductor)}$ and $R_{(Semiconductor)}$ with fill factor. The resistance values observed are typically very high when compared to others as the contact resistance comes into play. Hence, these resistance values are not of much significance unless the contact resistance is removed.

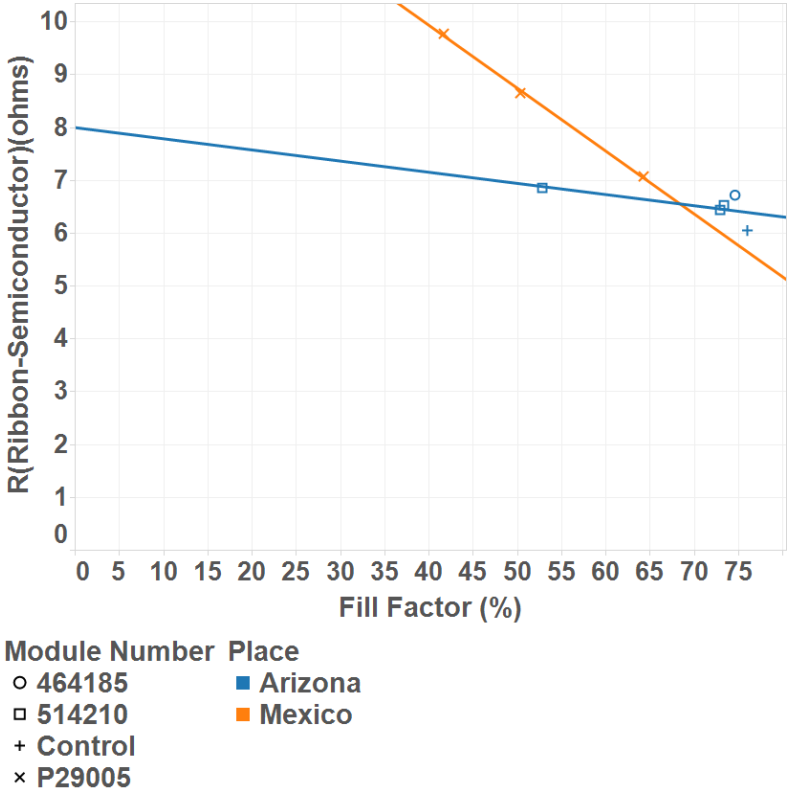

Figure 55: $R_{(Ribbon - Semiconductor)}$ Vs Fill Factor of Cells from Arizona and Mexico Aged Modules

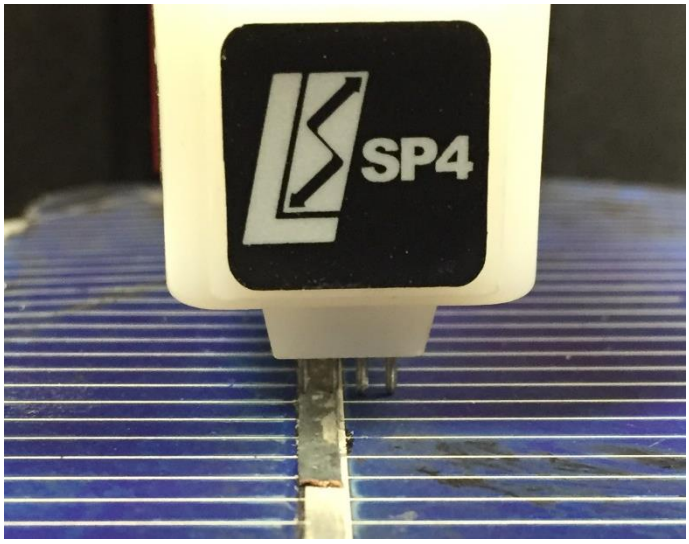

Figure 56: Placement of Four-Point Probe for Ribbon - Semiconductor Resistance Measurement

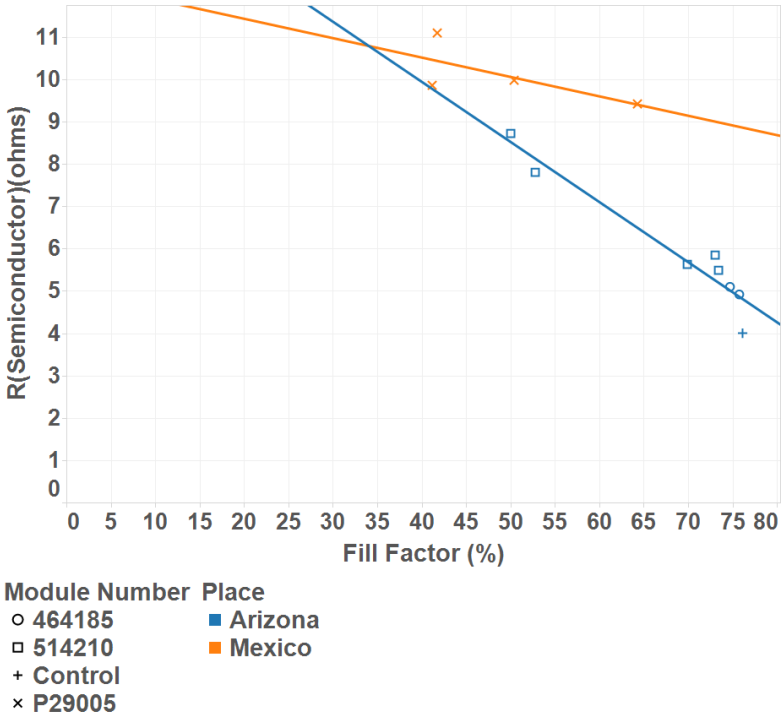

Figure 57: $R_{(Semiconductor)}$ Vs Fill Factor of Cells from Arizona and Mexico Aged Modules

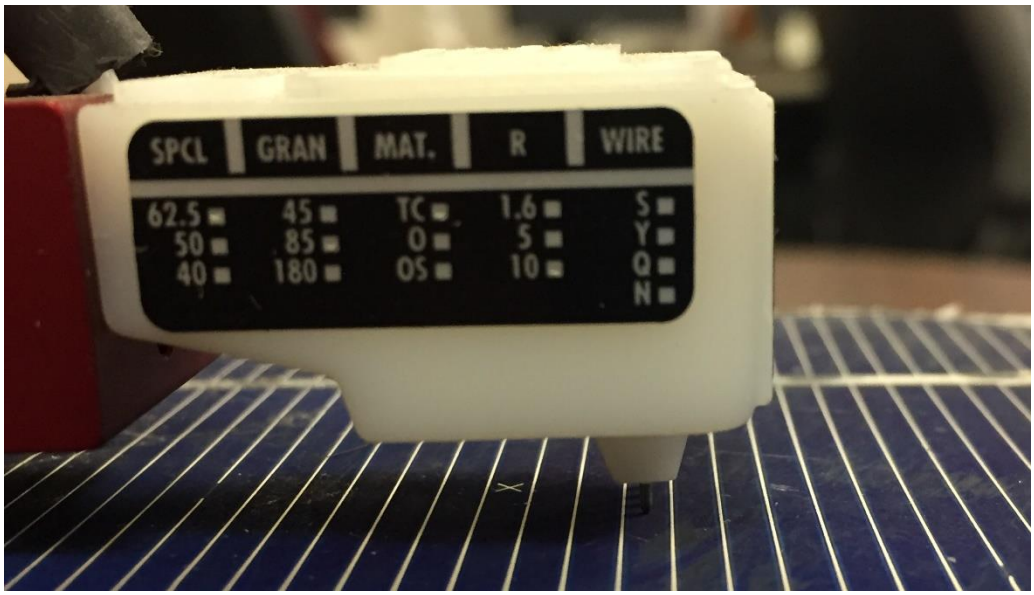

Figure 58: Placement of Four-Point Probe for Semiconductor Resistance Measurement

Table 4 shows the variation of different combinations of resistance for aged modules from Arizona and Mexico when compared to control module from Arizona.

Table 4:Comparison of Resistances of Aged Modules With Control Module

Combination	Control module (Ω)	Arizona modules (Ω)	% change	Mexico module (Ω)	% change
R (Semiconductor)	4.6	8.73	89.78 (↑)	11.1	141.3(↑)
R (Ribbon - Semiconductor)	6.045	6.88	13.81(↑)	9.77	61.62(↑)
R (Busbar - Solder)	0.0045	0.011	144.44(↑)	0.0143	217.77(↑)
R (Busbar - Semiconductor)	4.35	5.57	28.04(↑)	7.015	61.26(↑)
R (Ribbon- Busbar)	0.0052	0.0176	238.4(↑)	0.0171	228.8(↑)
R (Busbar - Fingers)	0.0212	0.0656	209.43(↑)	0.0235	10.84(↑)

It is to be noted that the control module for both Arizona and Mexico was assumed to be the same. It can be observed that the highest rise in resistance is observed for $R_{(Ribbon-Busbar)}$ which implies that the interface between the ribbon and busbar is the most effected interface resulting in power loss and fill factor drop. The second most affected resistance was determined to be the resistance of fingers-busbar part.

4.6 Climate Specific Thermal Modelling

This section mainly deals with the climate specific thermal modelling which is the calculated thermal fatigue accumulated over the years in a module a specific geographic location by using the weather data of that location. The thermal fatigue is caused by the daily temperature cycles that is due to the hot temperature of the module during the day and cold temperature during the night. Also, another major factor for the thermal fatigue is the cloud cycles during the day which cause sudden change in temperature which causes the sudden expansion and contraction of the solder bond and ribbons in the PV module. In this section, the thermal fatigue accumulated in modules from four different sites namely Arizona, California, Mexico and Colorado were calculated and were compared against other factors like peel strength and module level R_S obtained from dark I-V curves. Since the modules from each site are exposed for different number of years, for consistency purposes, the accumulated fatigue over the years 1991-2010 were considered for all the four sites even though the thermal fatigue was calculated throughout the time they were exposed in the field. The peel strength values represented in this section are the average load which is required to peel the ribbon from the cell.

These values were calculated by taking the average of the load from all cells from the aged modules of that particular climate.

Figure 59 shows the relationship between the module level R_S and the average peel strength of the same module obtained from different cells. Module level dark I-V was taken by passing the I_{SC} under dark conditions and the series resistance was calculated by taking the slope of the last few points at the V_{OC} side of the I-V curve. From the figure, it can be observed that the peel strength of the module decreases with increase in the series resistance of the module which is similar to the trend observed when peel strength was compared with cell level series resistance taken from dark I-V curves.

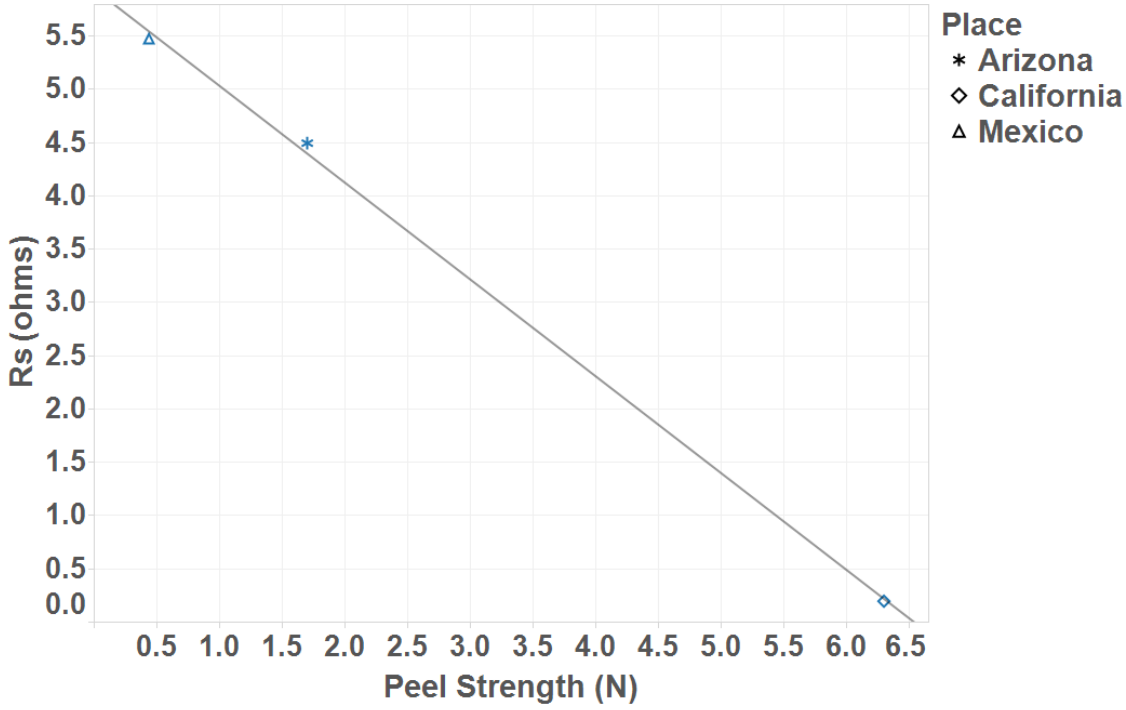

Figure 59: Module Level R_S Vs Peel Strength of Modules from Different Climates

Figure 60 shows the plot between the peel strength and thermal fatigue accumulated in the module over a period of 20 years from 1991-2010. It can be observed that peel

strength and fatigue have no correlation as such. It can be also concluded that lower fatigue does not imply higher bond strength. In order to fully demonstrate the absence of fatigue vs peel strength, it is recommended to pull one module every year from a plant from a single manufacturer in Arizona as there is no corrosion but only thermal fatigue and generate this plot again.

Peel strength is influenced by both material/design properties and process control as well. Since process control from one manufacturer to another manufacturer varies, no correlation between fatigue and peel strength could be expected.

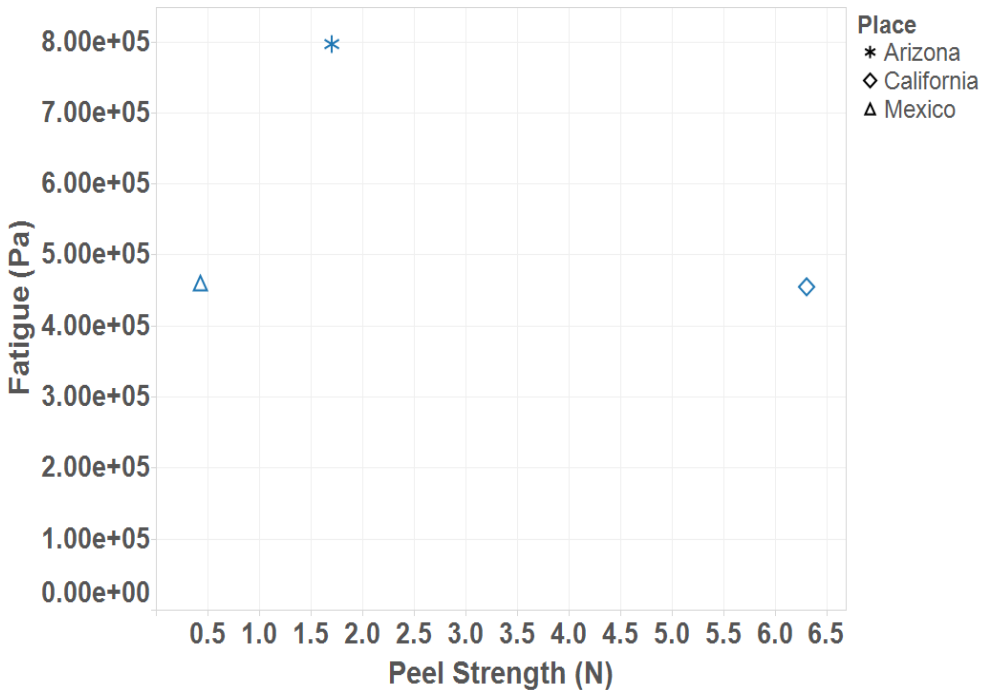

Figure 60: Peel Strength Vs Thermal Fatigue Accumulated 20 Years (1991-2010) Of Modules from Different Climates

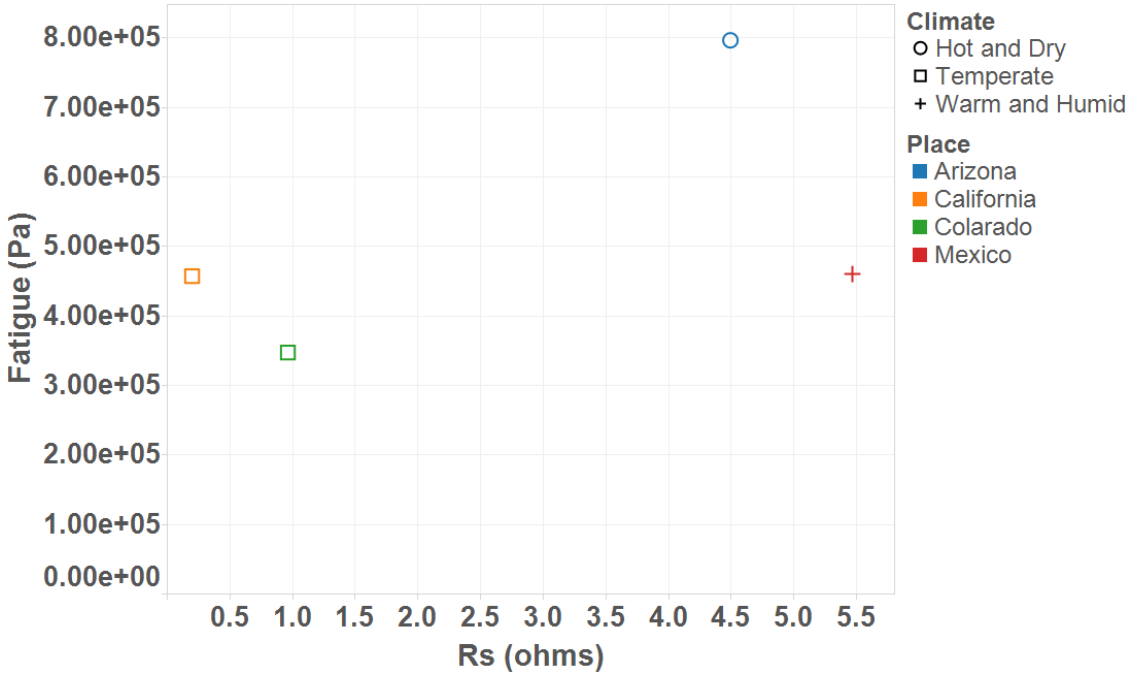

Figure 61: Module R_S Vs Thermal Fatigue Accumulated 20 Years (1991-2010) Of Modules from Different Climates

Figure 61 shows the relationship between the module level R_S and the thermal fatigue accumulated by the module over a span of 20 years from 1991-2010. From the plot it can be observed that typically higher thermal fatigue should lead to weakened bond strength due to temperature and cloud cycles which results in expansion and contraction of solder bonds and ribbons. This weakens the interface between ribbon-solder and ribbon-busbar resulting in higher series resistance. However, in the figure below, Mexico whose climate is warm and humid has the highest series resistance but not highest fatigue which implies that not only fatigue, but factors like corrosion can also aide the increase in series resistance in the presence of humidity/moisture.

5.0 CONCLUSIONS

The M55 photovoltaic modules of Arco/Siemens exposed in three climates (hot-dry, warm-humid and temperate) and aged between 18 and 28 years have been evaluated in this study. The test samples were extracted from these modules using the mechanical and chemical methods. The test samples were subjected to various experiments and the key conclusions obtained from these evaluations are listed below.

1. The fill factor and short-circuit current of the test samples are the most affected performance parameters. The fill factor is determined to be affected by the increase of series resistance and the short-circuit current is determined to be affected by the encapsulant browning and series resistance.
2. Temperature of the cell increases with the increase in series resistance. Also, the temperature along the solder in a cell was observed to be higher than the temperatures at the edge and center of the cells. In a module from Mexico where series resistance effect is higher, a 0.05 Ω increase in series resistance causes a 2.7^{o}C increase in temperature near the solder region when compared to 1.07^{o}C and 0.94^{o}C increase in edge and center regions, respectively.
3. Time for dissolution of ethylene vinyl acetate (EVA) using trichloroethylene solution is dictated by the weakening of interface between the encapsulant/glass or encapsulant/cell due to age, cloud cycles which includes sudden temperature changes and also mainly due to the presence of higher level of humidity in the atmosphere. This is the main reason why the EVA in the samples from Mexico dissolved at a much higher rate when compared to Arizona and California samples.

4. Two methods, namely chemical and mechanical methods, were developed in order to separate the cell from the glass and encapsulant of the modules. It was observed that the peel strength remains same for both methods thus indicating no change in properties of the solder bond due to the usage of TCE. Out of the two methods, the usage of mechanical method is best recommended as the experiment is non-hazardous and cost friendly. The downsides of mechanical method are its sample size and the time consumed. It is recommended to prepare the setup and leave it overnight so that metal piece bonds to the cell properly. The chemical method is a costly and hazardous method, and is only recommended to be used when a whole cell needs to be extracted from the module.
5. The peel strength of the ribbon-busbar interface decreases with increase in series resistance. The major factors that might influence the degradation of the interface are the cloud cycles which cause expansion and contraction of the ribbon which induces cracks in the solder bonds over the years and also corrosion when the module is fielded in humid conditions. For the module from Mexico, the peel strength decreases by 47% between the lowest series resistance cell and the highest series resistance cell. For Arizona, one module (464185) which has a series resistance of 1.4Ω had an average peel strength of 3.01N compared to another module (514210) which has a series resistance of 4.49 Ω had an average peel strength of 0.9N.
6. In the four-point probe resistance measurements, it was observed that the ribbon-busbar configuration was the major part effecting the series resistance and fill

factor. The resistance of the fingers remained nearly constant irrespective of the change in the fill factor.

7. Thermal fatigue developed by the modules over the years due to cloud cycles was investigated to observe if there is any correlation between thermal fatigue and peel strength. Since peel strength is influenced by both thermal fatigue and corrosion, no specific correlation between thermal fatigue and peel strength could be established. Mexico module, despite having a lower calculated fatigue, has a high series resistance which is possibly due to the moisture ingress through the backsheet or laminate edges leading to corrosion of metallic components of the cells.

6.0 REFERENCES

1. Pysch, D., Mette, A. and Glunz, S.W., *A review and comparison of different methods to determine the series resistance of solar cells.* Solar Energy Materials and Solar Cells, 2007. **91**(18): p. 1698-1706.

2. Quintana, M., et al. *Commonly observed degradation in field-aged photovoltaic modules*. in *Photovoltaic Specialists Conference, 2002. Conference Record of the Twenty-Ninth IEEE*. 2002. IEEE.

3. King, D., et al., *Photovoltaic module performance and durability following long-term field exposure.* Progress in Photovoltaics Research and Applications, 2000. **8**(2): p. 241-256.

4. Van Dyk, E. and Meyer, E., *Analysis of the effect of parasitic resistances on the performance of photovoltaic modules.* Renewable energy, 2004. **29**(3): p. 333-344.

5. Oh, C., et al., *Bonding copper ribbons on crystalline photovoltaic modules using various lead-free solders.* Journal of Materials Science: Materials in Electronics, 2015. **26**(12): p. 9721-9726.

6. Kim, T.H., Park, N.C., and Kim, D.H., *The effect of moisture on the degradation mechanism of multi-crystalline silicon photovoltaic module.* Microelectronics Reliability, 2013. **53**(9): p. 1823-1827.

7. Mallineni, J., *Failure and Degradation Modes of PV modules in a Hot Dry Climate*. 2013, Arizona State University.

8. Araujo, G.L. and Sanchez, E., *A new method for experimental determination of the series resistance of a solar cell.* IEEE Transactions on Electron Devices, 1982. **29**(10): p. 1511-1513.

9. Aberle, A., Wenham, S., and Green, M., *A new method for accurate measurements of the lumped series resistance of solar cells*. in *Photovoltaic Specialists Conference, 1993., Conference Record of the Twenty Third IEEE*. 1993. IEEE.

10. El-Adawi, M. and Al-Nuaim, I., *A method to determine the solar cell series resistance from a single I–V. Characteristic curve considering its shunt resistance—new approach.* Vacuum, 2001. **64**(1): p. 33-36.

11. Rauschenbach, H., *Solar cell array design handbook-The principles and technology of photovoltaic energy conversion.* NASA STI/Recon Technical Report A, 1980. **80**: p. 34847.

12. Agarwal, S., et al., *A new method for the measurement of series resistance of solar cells.* Journal of Physics D Applied Physics, 1981. **14**: p. 1643-1646.

13. Bashahu, M. and Habyarimana, A., *Review and test of methods for determination of the solar cell series resistance.* Renewable energy, 1995. **6**(2): p. 129-138.

14. Dubey, R., et al. *Performance degradation in field-aged crystalline silicon PV modules in different Indian climatic conditions*. in *2014 IEEE 40th Photovoltaic Specialist Conference (PVSC)*. 2014. IEEE.

15. Bosco, N., Silverman, T. J., and Kurtz, S., *Climate specific thermomechanical fatigue of flat plate photovoltaic module solder joints.* Microelectronics Reliability, 2016.

16. Chicca, M. and TamizhMani, G., *Nondestructive techniques to determine degradation modes: Experimentation with 18 years old photovoltaic modules*. in *Photovoltaic Specialist Conference (PVSC), 2015 IEEE 42nd*. 2015. IEEE.

17. Packard, C.E., Wohlgemuth, J.W., and Kurtz, S.R., *Development of a visual inspection data collection tool for evaluation of fielded PV module condition*. 2012, National Renewable Energy Laboratory (NREL), Golden, CO.

18. Doi, T., et al., *Experimental study on PV module recycling with organic solvent method.* Solar energy materials and solar cells, 2001. **67**(1): p. 397-403.